Spatial variability of seasonal precipitation lapse rates in complex topographical regions - application in France

Valentin Dura[1,2], Guillaume Evin[2], Anne-Catherine Favre[2], and David Penot[1]

[1]EDF-DTG, Grenoble, France
[2]Univ. Grenoble Alpes, INRAE, CNRS, IRD, Grenoble INP, IGE, 38000 Grenoble, France

Correspondence: Valentin Dura (valentin.dura@edf.fr)

Abstract. Seasonal precipitation estimation in ungauged mountainous areas is essential for understanding and modeling a physical variable of interest in many environmental applications (hydrology, ecology, cryospheric studies). Precipitation Lapse Rates (PLRs), defined as the increasing or decreasing rate of precipitation amounts with the elevation, play a decisive role in high-altitude precipitation estimation. However, the documentation of PLR in mountainous regions remains weak even though their utilization in environmental applications is frequent. This article intends to assess the spatial variability and the spatial-scale dependence of seasonal PLRs in a varied and complex topography region. At the regional scale (10,000 km^2), seven different precipitation products are compared in their ability to reproduce the altitude dependence of the annual/seasonal precipitations of 1,836 stations located in France. The Convection-Permitting Regional Climate Model (CP-RCM) AROME is the best in this regard, despite severe precipitation overestimation in high altitudes. The fine resolution of AROME allows for a precise assessment of the influence of altitude on winter and summer precipitations on 23 massifs at the sub-regional scale ($\sim$ 1,000 km^2) and 2,748 small catchments ($\sim$ 100 km^2) through linear regressions. With AROME, PLRs are ~~mostly~~ often higher in winter at the catchment scale. The variability of PLR is higher in high-altitude regions such as the French Alps, with higher PLRs at the border than inside the massifs. This study emphasizes the interest of conducting PLR investigation at a fine scale to reduce spatial heterogeneity in the seasonal precipitations–altitude relationships.

1 Introduction

Precipitation Lapse Rates (PLRs) refer to the increasing or decreasing rate of precipitation amounts with elevation. The rise of moist air above an orographic barrier such as hills or mountains generates precipitations that affect the ice cover and the precipitation amount contained in snowpacks (Bales et al., 2006; Viviroli et al., 2007; Mott et al., 2014; Dozier et al., 2016; Wrzesien et al., 2019). Therefore PLR is the main factor that controls the water budget of high-altitude catchments (Jiang, 2003) and partly explains the freshwater supply in the summer season. On shorter time scales like hourly or daily scales, PLRs help understand the physical mechanisms of orographic precipitations responsible for natural hazards such as avalanches, landslides, and floods (Caracena et al., 1979; Caine, 1980; Conway and Raymond, 1993; Buzzi et al., 1998; Panziera et al., 2015). PRLs can also be of importance for hydrological modeling, for which precipitation inputs are often spatialized with geostatistics models (Daly et al., 1994; Gottardi, 2009; Frei and Isotta, 2019) or can be distributed by altitudinal bands using assumed

25 PLR values (Bergström, 1992; Ragettli and Pellicciotti, 2012; Markstrom et al., 2015; Garavaglia et al., 2017; Ruelland, 2020; Kumar et al., 2022) to complete the hydrological balance (Oudin et al., 2006) in high-altitude catchments. The investigation of PLR is a topical and crucial issue in multiple domains such as energy production, agriculture, tourism, condition of ecosystems, risk management (Pimentel et al., 1997; Gössling et al., 2012).

The relationship between altitude and precipitation accumulation is not straightforward on small-time scales and depends
30 on precipitation type (stratiform *vs* convective), wind, and flow directions (Sevruk and Mieglitz, 2002; Schäppi, 2013). PLR at the hourly scale may even exhibit a negative trend during extreme events (Formetta, 2021) due to the drying of the air mass. When aggregated over extended periods, the relationship between precipitation and elevation becomes simpler to model, with generally a precipitation increase as elevation increases (Barrows, 1933; Spreen, 1947; Schermerhorn, 1967; Smith, 1979). However, PLR values can differ among seasons and regions due to different weather processes (Napoli et al., 2019; Ménégoz
35 et al., 2020). In the Alps, large-scale processes mainly generate winter precipitation. Convective processes are more frequent in summer.

In a hydrology framework, PLRs refers to the slope of the linear regression between precipitation and elevation on spatial areas (e.g. Sevruk, 1997; Gottardi, 2009; Ogrin and Kozamernik, 2020; Avanzi et al., 2021; Bell et al., 2022) rather than on vertical atmospheric columns. In some cases, the relationship in high-altitude regions appears to be non-linear with a threshold
40 impact (Schäppi, 2013; Napoli et al., 2019) due to the drying of the air masses, and the use of quadratic regression is then recommended (Mahmood et al., 2021).

PLRs are often estimated from ground measurements from rain gauges, observations of Snow Water Equivalent (SWE) (Avanzi et al., 2021) derived from manual coring or radiation, and snow/rain gauges totalizator (Gottardi, 2009) measures. Using only ground stations to estimate PLRs requires a sufficient coverage of high-elevation areas, which is rarely met in
45 practice (Hofstra et al., 2010). High-elevation stations are prone to precipitation under-catch (Groisman and Legates, 1994; Pollock et al., 2018) and snow-redistribution. Strong winds coupled with a significant amount of solid precipitation might even induce an annual underestimation of up to 25% (Sevruk, 1997). Moreover, the robustness of the regressions and the local influences of altitude on precipitation must be balanced because of the irregular spatial sampling of punctual observations (Gottardi, 2009). In practice, in sparse rain gauge regions, PLR can only be computed on vast areas and fails to reflect the local
50 relationship between altitude and precipitation.

As an alternative, gridded precipitation products can help analyze the spatial variability of PLR at a fine spatial scale. Radar products that indirectly measure precipitation from reflectivity have been extensively used in hydrology (e.g. Ochoa-Rodriguez et al., 2019). However, radar data are inherently biased in mountainous regions due to ground echoes and beam blockage (e.g. Berne and Krajewski, 2013), which results in an underestimation of PLR (Faure et al., 2019). Satellite precipitation products,
55 despite certain limitations, are another easily accessible source of data. The biases in mountain regions and the relatively low resolution of the data present challenges in calculating PLR from satellite data (Li et al., 2017). Composite products merging radar or satellite to rain gauge data (Champeaux et al., 2009; Nie et al., 2015; Nguyen et al., 2020) can also be an option for the assessment of PLRs. However, the latter products are sensible on the density of the rain gauge network and suffer where no rain gauge are available (Silverman et al., 2013; Shen et al., 2018; Frei and Isotta, 2019). Regional Climate models (RCM) have

been used in numerous studies to evaluate the variability of PLR at regional scales (e.g. Kotlarski et al., 2012; Cuo and Zhang, 2017; Ménégoz et al., 2020). All results show that PLRs obtained with RCM data are larger and more spatially varying than those using rain gauges. Convection-Permitting Regional Climate Models (CP-RCMs) have recently emerged as an appealing tool for producing fine-resolution ($1 - 4\,\mathrm{km}^2$) climate simulations (Rockel et al., 2008; Brousseau et al., 2016; Keuler et al., 2016; Belušić et al., 2020). CP-RCMs are a refined extension of RCM where deep convection parametrization, a dominant source of precipitation error (Hohenegger et al., 2008; Foley, 2010; Kendon et al., 2012), is turned off. To produce a long series of CP-RCM simulations, including precipitation, a Numerical Weather Prediction (NWP) model is often driven by a RCM or a satellite-based reanalysis. CP-RCMs produce better precipitation intensities and frequencies than RCMs during heavy events (Ban et al., 2021; Caillaud et al., 2021). CP-RCMs represent more accurately orographic precipitation than RCMs because they explicitly resolve deep convective processes and include a finer representation of the topography (Lucas-Picher et al., 2021). These improvements occur especially in summer when convective events play a major role (Ban et al., 2021). Today, CP-RCMs are considered more reliable than reanalysis (Lundquist et al., 2019) in ungauged mountainous areas, despite current precipitation overestimation (Gerber et al., 2018; Dallan et al., 2023).

This paper explores the spatial variability of winter and summer PLR across a complex topographical region, with a dense network of 1,836 stations used as ground truth. The first objective is to compare seven types of gridded products (interpolator, reanalysis, satellite, radar, CP-RCM) in their ability to capture the relationship between observed annual/seasonal precipitations and altitude. The second goal is the investigation of the spatial variability of winter and summer PLR values at the sub-regional ($\approx 1,000\,\mathrm{km}^2$) and catchment ($\approx 100\,\mathrm{km}^2$) scales using a gridded precipitation product without ground station assimilation. Nesting of catchments in sub-regions allows the study of the spatial-scale dependence of PLR to provide guidelines for future precipitation interpolation studies. To our knowledge, only Jiang et al. (2022) explores these questions in the Third Pole. In a sparse rain gauge region, the authors found an accurate PLR reproduction with downscaled ERA5 precipitation product (Jiang et al., 2021). They highlighted the spatial variability of PLR at the catchment scale and emphasized the importance of conducting PLR studies at the finest possible spatial scale.

This paper is organized as follows. Section 2 describes the study domain and the available precipitation products. Section 3 presents the method used to derive PLR. Section 4 shows the results of the reproduction and spatial variability of PLR by the different products considered. Section 5 compares the findings to the literature and discusses some perspectives. Section 6 gives the conclusions.

2 Domain and data under study

2.1 A complex mountainous region

Figure 1(**a**) shows the study domain, which corresponds to the intersection of the spatial extents of the seven gridded precipitation products. The topography of the region is complex and varied, including three major mountain chains: the Alps, the Pyrénées, and the Massif Central. The Massif Central is a mid-mountain range reaching 1,885 m in the center of the Southern half of France and covers 85,000 km^2, which makes it the largest mountainous region of the country (15 % of the total surface

area of France). The Massif Central is bordered by the Rhone Valley in its Western part and the Mediterranean coastal plain in its Southern part. This region is mainly composed of large plateaus ranging in altitude from 600 m to 900 m and enclosed by mountains with circular summits corresponding to extinct volcanoes. The altitude presents an asymmetrical profile with summits in the South and the East (Cévennes) and less elevated areas in the northwest. The landscapes are varied and contain limestone plateaus cut by deep canyons, mountain peaks, and deep river valleys. The Massif Central is exposed to the Western wind and captures the precipitation coming from the Atlantic Ocean.

The Alps are the highest mountain range in Europe, reaching 4,808 m at the Mont-Blanc. The chain has a 40,000 km^2 surface area and is 1,200 km long, crossing seven countries: France, Switzerland, Italy, Germany, Liechtenstein, Austria, and Slovenia. The French Alps are separated from the Massif Central by hills and are divided into the Northern and the Southern parts. The Northern Alps are higher and have large valleys. In the Southern Alps, valleys are narrower. The climate of the French Alps has three main influences. The moist air can come from the West Atlantic. The warm air comes from the Mediterranean and blows Northward. ~~Mediterranean circulation from Italy phenomenon (Garavaglia et al., 2010) brings~~ In winter, easterly weather fronts coming from the Italian Alps can bring large amounts of ~~snow in the most Easterly regions during the winter.~~ precipitation in the east of the French Alps (Garavaglia et al., 2010). Generally, these meteorological events do not reach the foothills of the French Alps. The Northern Alps are more rainy than the Southern Alps, which have almost 300 days per year of sunshine. The French Alps is a territory of high altitude and complex topography. The ~~significative~~ significant variations in mountain elevation and exposure result in the coexistence of multiple climates at small spatial scales. Mountains create micro-climatic conditions and influence daily weather. The Jura is a sub-alpine mountain range located in the North of the French Alps. It covers a surface area of 5,000 km^2 and reaches 1,700 m. It is a mid-mountain range composed of plateaus with a mean altitude of 600 m.

The Pyrénées form a natural border between France and Spain by joining the Atlantic Ocean to the Mediterranean Sea over 430 km long. It covers 19,000 km^2 and reaches 3,200 m on the French side, making it the second-highest mountain range in France. Most valleys are running South-North. The Spanish part is more arid and rocky than the French part, which catches the precipitation from the Atlantic. The French Pyrénées splits into the Atlantic, Central, and Eastern parts. The relief rises steeply from sea level to hills in the Atlantic and Eastern parts. The Central Pyrénées host sharp peaks but are more rounded than the Alps because of erosion. The Atlantic part gets more precipitation because of rainy Northwest winds. The wind from the Southwest brings warmer air in summer. The topography is diverse, with snow-capped mountains, deep green valleys, and coastal hills. The remaining of France consists of plains and are not included in this study.

In this study, we consider three spatial scales: the regional scale (10,000 km^2), the sub-regional scale (1,000 km^2), and the catchment scale (100 km^2). ~~PLR computation will be conducted at the~~ The sub-regional ~~(massif) and catchment scales so it can have a hydrologic interpretation~~scale consists of areas named "massif", which form a set of continuous reliefs, often separated by rivers and valleys. An ensemble of massifs constitutes a mountain range (Alps, Pyrenees). In the French Alps, 23 ~~sub-regions named "massifs "~~massifs have been identified through climatological homogeneity of precipitation in Pahaut (1991). PLR computation will be conducted at the massif (climatological homogeneity) and catchment (hydrologic interpretation) scales. The surface areas of the massifs range from 450 to 1,600 km^2, with a median value of 870 km^2. The

2,748 catchments collected from Sandre (2020) have a mean surface area ranging from 0.009 to 1,000 km^2, with a median value of 100 km^2. Figure 1(**c**) illustrates the massifs and the catchments analyzed in this study. The altitude is represented with a digital terrain model of 1 km resolution. The study domain is divided into squares of 1 km^2 that are referred to as "pixels".
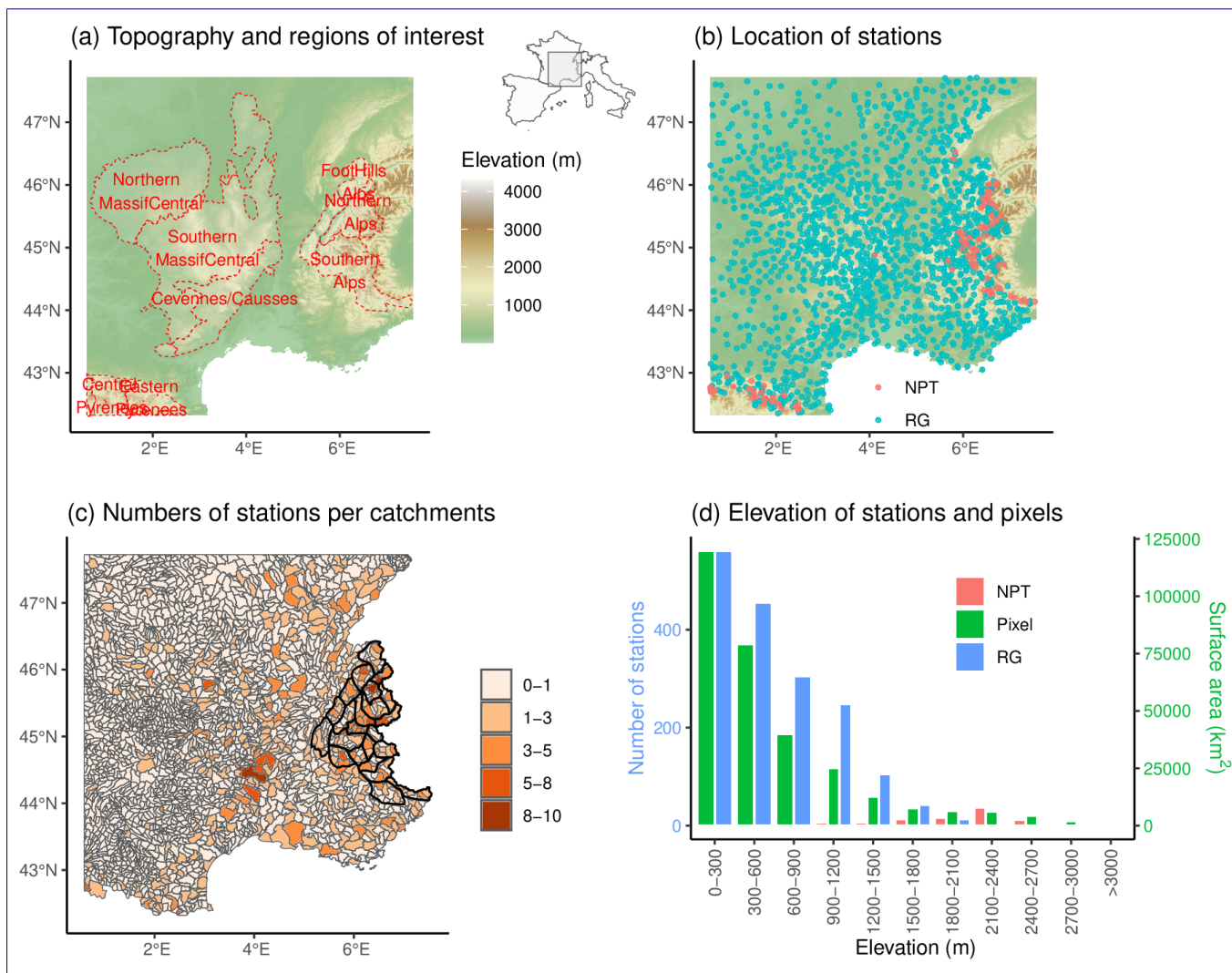
Figure 1. (**a**) Topography of France and boundaries of eight sub-regions of interest. The extent of the study domain is located in France and is bordered by Spain, Italy, and Switzerland. (**b**) Location of stations, blue points refer to rain gauges (RG) and red points to NPT (see subsection 2.2). (**c**) Catchments and the corresponding number of stations. Boundaries of massifs located in the Alps are also indicated in black. (**d**) Histogram of the altitude of stations (rain gauges (RG), and NPT) and of the covered surface area (in green).

2.2 A dense network of stations

Figure 1(**b**) presents the dense rain gauge network of 1,836 stations used in this study, with an average density of one rain gauge per 160 km^2. Electricité de France (EDF, the main electricity provider in France) and Meteo-France provide 673 and 1,163 stations, respectively. We aggregate available daily precipitation data to obtain seasonal and annual precipitation. Figure 1(**d**) shows the number of rain gauges per altitudinal band. A small number of rain gauges is available above 2,000 m, causing an under-representation of high-altitude regions. To overcome this limitation, EDF has implemented a snow rain gauges totalizator (Nivo Pluviomètre Totalisateur, NPT in French) device (Gottardi, 2009). NPTs collect annual precipitation in a small orifice protected from the wind by a large collar. Snow falling in the orifice feeds a reservoir containing a saline solution able to melt solid precipitation. The operating period ranges from 1945 to 1977 and differs among NPTs. We restricted the period to 1957–1973, where the spatial density of NPT is at its maximum. An exploratory analysis of the annual precipitation from NPTs removes outliers and missing values. Following this analysis, we keep 130 NPTs among 216 for the study. NPTs are primarily found in the Mont-Blanc region and are more uncommon, for instance, in the center of the Pyrénées. Figure 1(**c**) illustrates the irregular number of weather stations per catchment. Mountainous regions like the Alps and the Cévennes are more covered than plains, where weather processes are less subject to spatial variability. Nevertheless, the Southern Alps, the Massif Central, and the Pyrénées have a complex topography and few stations. The sparse stations in some mountainous regions and their location in valleys largely constrain the ability to compute PLR using only precipitation aggregated from rain gauges.

In France, precipitation patterns differ among seasons. Thus in this study, four seasons are considered: winter (December, January, February (DJF)), spring (March, April, May (MAM)), summer (June, July, August (JJA)), and autumn (September, October, November (SON)).

2.3 Gridded precipitation products

This study explores the ability of multiple gridded precipitation products to assess the relationship between annual precipitation and altitude. Precipitations from gridded products are available at daily, hourly, or sub-hourly timescales and aggregated to obtain seasonal precipitations. These products are briefly described hereafter and are summarized in Table 1.

2.3.1 ERA5-Land

ERA5-Land (Muñoz-Sabater et al., 2021) is a global reanalysis that operates by simulating atmospheric and surface variables, including hourly precipitation. It uses the ERA5 atmospherical fields downscaled with linear interpolation at the resolution of 9 km. ERA5-Land assimilates satellite data and does not rely on rain gauges. The quality of ERA5-Land precipitation is dependent on the density of satellite and radar networks used in the assimilation process (Hassler and Lauer, 2021). As a result, the quality is better in Central Europe and the U.S. than in tropical oceans. The improved horizontal resolution of 9 km compared to 31 km (ERA5) or 80 km (ERA-Interim) is a benefit of ERA5-Land (Muñoz-Sabater et al., 2021). This results in a better representation of spatial precipitation patterns (Gomis-Cebolla et al., 2023).

2.3.2 CERRA-Land

Copernicus European Regional ReAnalysis Land (CERRA-Land) (Le Moigne, 2021) is the most up-to-date reanalysis available in Europe since September 1984 at a horizontal resolution of 5.5 km. It uses ERA5 as lateral boundary conditions to run the

165 atmospherical model HIRLAM ALADIN Regional/Mesoscale Operational NWP In Europe (HARMONIE) every 3 hours at a native resolution of 5.5 km. The analysis is given to the MESCAN system (Soci et al., 2016) to produce daily precipitation fields by merging it with nearly 8,000 daily rain gauge measurements through optimal interpolation. Le Moigne (2021) found that CERRA-Land leads to a better representation of the seasonality of snow depth in the Alps compared to ERA5-Land.

2.3.3 PDIR-NOW

170 PERSIANN Dynamic Infrared-Rain Rate (PDIR-NOW, Nguyen et al., 2020) is a satellite-based product using high-frequency (15 min) sampled infrared imagery, at a 4 km spatial resolution. PDIR-NOW estimates precipitation based on empirical cloud-top temperature–precipitation rate relationships. Errors resulting from this method are corrected by calibrating the empirical relationships regionally based on monthly precipitation climatology. PDIR-NOW has better diurnal cycle representation, rain/no rain days estimation, and regional precipitation patterns compared to the other PERSIANN family products (Nguyen

175 et al., 2020). The inter-annual, annual, and seasonal precipitations are less biased with PDIR-NOW (Huang et al., 2021; Uysal, 2022). In the following, PDIR-NOW will be referred to as PDIR.

2.3.4 SERVAL

The *Système d'élaboration des produits radar et de visualisation centralisé* (SERVAL, previously PANTHERE, Champeaux et al., 2009) product provides precipitation amounts at a frequency of 5 minutes and a spatial resolution of 1 km by merging

180 individual radar fields. Before any radars are combined, each one is individually calibrated using data from hourly rain gauges, with a mean hourly correction ratio applied uniformly across the whole radar coverage. If a pixel falls under the coverage of multiple individual radars, the selected precipitation corresponds to the maximum of precipitation seen by the considered radars. As already mentioned, radars are affected by many sources of potential errors, such as beam blocking and ground echoes. ~~A precipitation probability product based on cloud classification filters clear air and ground echoes~~Ground echoes are

185 removed using pixel precipitation probabilities, which are derived from a cloud classification filter. Bright band and signal attenuation phenomena are also corrected.

2.3.5 COMEPHORE

The *COmbinaison en vue de la Meilleure Estimation de la Précipitation HOraiRE* (COMEPHORE, Champeaux et al., 2009) is a precipitation reanalysis based on the combination of the previous SERVAL product with a dense rain gauges data set of

190 more than 4,000 observations. Kriging of the rain gauge values is applied to obtain the stratiform part, while the convective part involves the radar precipitation re-calibration with the rain gauge amounts. The main idea underlying this product is to combine the coherent spatial structure of the radars with the accuracy of rain gauge measurements to provide an hourly precipitation

field at 1 km resolution. COMEPHORE underestimates mountains annual precipitation (Rouzeau, 2013; Roger, 2017) since the altitude is not considered at any modeling stages. ~~Most radars have been integrated since 2006, and others have been gradually incorporated since 2015 to fill the gaps of measures in mountainous regions (Beck and Bousquet, 2013). The use of SERVAL and COMEPHORE is therefore tainted with temporal non-homogeneity.~~

2.3.6 SPAZM

The *SPAtialisation en Zones de Montagne* (SPAZM, Gottardi, 2009) is a precipitation interpolator that integrates rain gauge values with a meteorological guess conditioned by topography, and the weather type of the day. Eight weather situations are identified based on geopotential fields (Garavaglia et al., 2010) and eight corresponding mean daily precipitation fields are created through local linear regression between mean daily observed precipitation at stations and altitude, at the daily timescale and 1 km resolution. For a given day, the corresponding mean daily precipitation field is modified using the precipitation of the current day. SPAZM incorporates 2,201 various stations from EDF (rain gauges and NPT), Meteo-France, MeteoSwiss, Arpa Piemonte, and Instituto Nacional de Meteorología (INM) networks. SPAZM used fewer but higher stations than COMEPHORE. Its ability to provide accurate estimates of yearly precipitation makes it a valuable tool for hydrological applications (Gottardi, 2009; Ménégoz et al., 2020; Ruelland, 2020).

2.3.7 CNRM-AROME

The CNRM-AROME model is a CP-RCM based on the nonhydrostatic, convective-scale, limited-area model called *Applications de la Recherche à l'Opérationnel à Méso-Echelle* (AROME) used for the national weather prediction by Meteo-France since 2008 (Seity et al., 2011; Brousseau et al., 2016). 37 years of CNRM-AROME simulations are available at a horizontal resolution of 2.5 km, at the hourly timescale (Caillaud et al., 2021), for an Alpine domain defined in the Flagship Pilot Study of the Coordinated Regional Climate Downscaling Experiment (CORDEX-FPS, Coppola et al., 2020). The Atlantic Pyrénées are not contained in the domain. The version of AROME applied to obtain this long simulation is related to cycle 41t1 (Termonia et al., 2018) and corresponds to the version in operational use at Meteo-France, between December 2015 and December 2017. In the remainder of the paper, CNRM-AROME CP-RCM will be referred to as AROME. The initial atmospheric conditions of AROME are provided every hour by a CNRM-ALADIN RCM simulation, itself driven by the ERA-Interim reanalysis. The fine resolution of the model enables a good representation of the deep convection scheme despite the absence of data assimilation. Precipitation from this version has been evaluated recently in multiple studies (Ban et al., 2021; Caillaud et al., 2021; Monteiro et al., 2022). Heavy precipitations are better represented than in the RCM CNRM-ALADIN but suspicious snow accumulation is pointed out in high altitudes. A first pre-processing stage is required to address large errors in precipitation seasonal amounts at the pixel scale. An iterative technique is applied to deal with the problematic pixels, whereby the abnormal values are replaced with the weighted (according to the altitude) average of the precipitation amount of the nearby pixels. A pixel is qualified as problematic if a difference of more than 500 mm in seasonal precipitations is noticed compared to a neighboring pixel.

225   Some gridded precipitation products present non-homogeneous data because of their large temporal depths. Most radars have been integrated since 2006, and others have been gradually incorporated since 2015 in mountainous regions (Beck and Bousquet, 2013). The use of SERVAL and COMEPHORE is therefore tainted with temporal non-homogeneity. Station density also affects the temporal homogeneity of COMEPHORE, CERRA-Land, and SPAZM. Changes in instrumentation have been corrected in COMEPHORE and SPAZM with homogenization of rain gauge precipitation (Gottardi, 2009; Mestre et al., 2013).

Table 1. Summary of the characteristics of the gridded precipitation products used in this study, namely available period, domain, horizontal resolution, frequency, type of observations, provider, and reference.

	Available period	Domain	Horizontal resolution	Frequency	Type of observations	Provider	Reference
ERA5-Land	1950–2023	World	9 km	Hourly	Reanalysis ECMWF replay	ECMWF	Muñoz-Sabater et al. (2021)
CERRA-Land	1984–2023	Europe	5.5 km	Daily	Reanalysis	C3S	Le Moigne (2021)
PDIR	2000–2023	60°N to 60°S	4 km	Hourly	Reanalysis Satellite	CHRS	Nguyen et al. (2020)
SERVAL	2006–2020	France	1 km	5min	Radar	Météo-France	Champeaux et al. (2009)
COMEPHORE	2007–2020	France	1 km	Hourly	Reanalysis Rain gauges + radar	Météo-France	Champeaux et al. (2009)
SPAZM	1950–2020	France	1 km	Daily	Reanalysis Rain gauges	EDF	Gottardi (2009)
AROME	1982–2018	Pan-Alps	2.5 km	Hourly	CP-RCM	Météo-France	Caillaud et al. (2021)

230   Figure 2 displays the mean annual precipitation for all gridded precipitation products. Fig. S1 in the Supplements provides the same information on a seasonal basis. We first notice the effect of the resolution. Annual precipitations from ERA5-Land and PDIR are very smooth on the considered domain compared to the other gridded products available at a finer resolution. The precipitation difference between plains and mountains is not very prominent in the radar products SERVAL and COMEPHORE. Comparatively, the Pyrénées, the Massif Central, and the Alps receive more annual precipitation with AROME, CERRA-Land,

235   and SPAZM. SPAZM leads to marked patterns in the alpine valleys and produces a higher correlation to altitude. AROME gives a large amount of precipitation in mountains, especially in the Massif Central. The seven gridded precipitation products show different precipitation amounts, especially in mountainous regions, due to more or less fine horizontal resolutions, different types of assimilated data, and differences in the treatment of the altitude effect.

3   Methods

240   Let $Pobs$ and $Pgrid$ denote respectively the observed (by rain gauges and NPT) and gridded precipitation (annual or seasonal) expressed in mm. Let Z indicate the altitude in m. The indices i and j refer to stations while the index p indicates the pixels.

3.1   Description of the relationship between precipitation and altitude

Annual and seasonal precipitations from the gridded products are extracted at station locations to evaluate the reproduction of the altitudinal variability of precipitation. The precipitations from the NPT are only available at the annual scale. The stations

245   are grouped by regions defined in Fig.1(**a**) and by 300-meter elevation bands b_{alt} ranging from 0–300 m to 3000–3300 m. For each elevation band and region, the median of observed ($Pobs_{b_{alt}}$) and gridded ($Pgrid_{b_{alt}}$) precipitation (annual and seasonal)
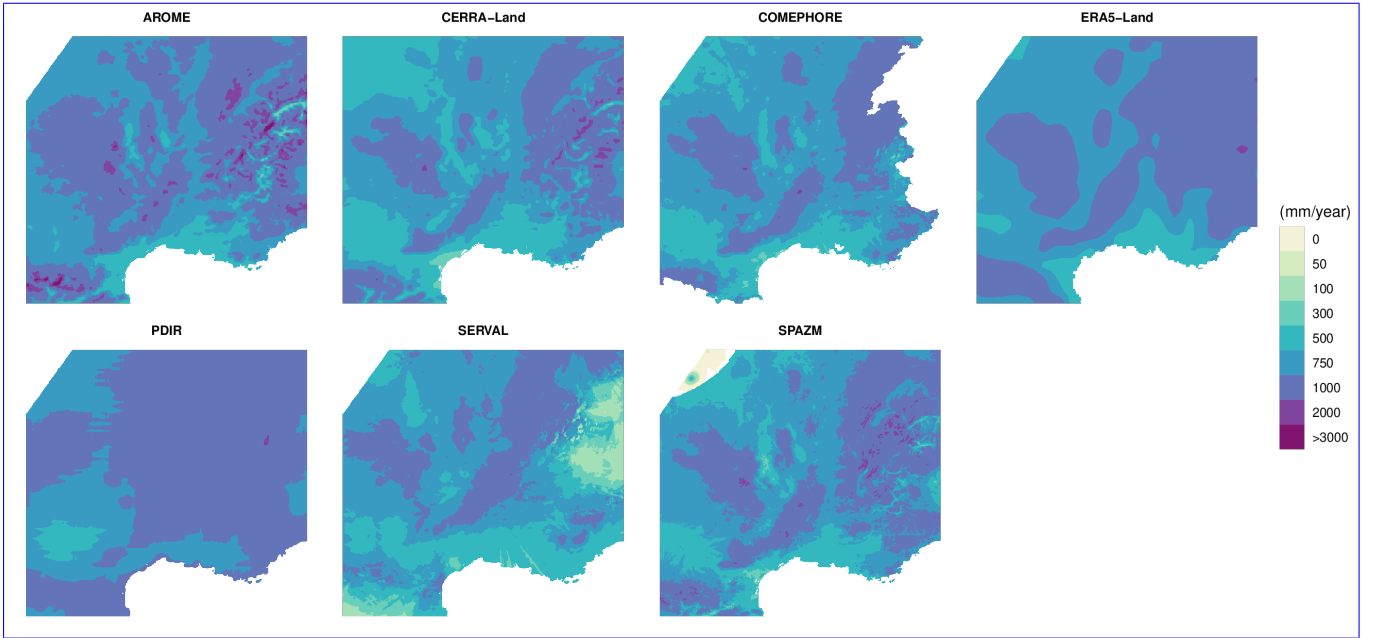
Figure 2. Mean annual precipitation for the gridded precipitation products (AROME, CERRA-Land, COMEPHORE, ERA5-Land, PDIR, SERVAL, SPAZM), on the period 2007–2017. ~~An upper limit of 4,500 mm has been fixed for better visibility but values can be higher.~~

is computed using all the locations of the stations belonging to this region and elevation band:

$$Pobs_{b_{alt}} = \hat{Pobs}_{i_{50\%}}, i \in b_{alt}, \qquad (1)$$

$$Pgrid_{b_{alt}} = \hat{Pgrid}_{i_{50\%}}, i \in b_{alt}. \qquad (2)$$

250   The median values should represent the considered region and elevation band and be unaffected by anomalous values resulting from a specific station location. A compromise between a high number of rain gauges per band and a sufficient number of bands led to a 300 m bandwidth selection. The bands with fewer than five rain gauges are not displayed in Fig.3**(a)** to prevent any misunderstandings or misrepresentations. To study the behavior of gridded precipitation products in high altitudes where no rain gauges are available, we compare the median of seasonal precipitations $\hat{Pgrid}_{p_{50\%}}, p \in b_{alt}$ extracted from pixels within

255   the altitudinal bands.

To test a gridded precipitation product in reproducing the spatial variability of the relationship between seasonal precipitations and altitude at a finer scale, we also compute Precipitation Relative Difference (PRD) for several couples of close neighboring stations with sufficient elevation difference. The two stations should have a separation distance lower than 20 km and have an elevation difference superior to 100 m. PRD should not be assimilated to Precipitation Lapse Rates (PLR) calcu-

260   lated at the catchment scale, see subsection 3.2. For the neighbouring stations i and j, we compute PRD at station locations for

observed ($PRD_{Pobs_{ij}}$) and gridded ($PRD_{Pgrid_{ij}}$) precipitation :

$$PRD_{Pobs_{ij}} = 100 \times 100 \times \frac{Pobs_i - Pobs_j}{Z_i - Z_j} \bigg/ \frac{Pobs_i + Pobs_j}{2} \ , \tag{3}$$

$$PRD_{Pgrid_{ij}} = 100 \times 100 \times \frac{Pgrid_i - Pgrid_j}{Z_i - Z_j} \bigg/ \frac{Pgrid_i + Pgrid_j}{2} \ . \tag{4}$$

The gradient of seasonal precipitations relative to the altitude is divided by the mean precipitation of the two stations and multiplied one time by 100 to get the result in percentage relative to the mean precipitation. This result is again multiplied by 100 to express PRD in percentages per hundred meters (%/100 m).

3.2 Regression at nested spatial scales

The primary focus of this study is the investigation of the spatial variability of seasonal PLRs at the sub-regional and catchment scales. It is possible to use stations at the regional scale, but the PLRs would be too dependent on their spatial sampling at the sub-regional and catchment scales. Indeed, some catchments contain zero or only one station (Fig.1(**c**)). As an alternative, we propose to use AROME to study the spatial variability of PLR at the sub-regional and catchment scales. The choice of AROME will be motivated in subsection 4.1. We assume linear relationships between seasonal precipitations and altitude. This strong hypothesis will be discussed later in subsection 4.3. The PLRs are calculated with linear regression between seasonal precipitations and altitude, expressed as follows:

$$Parome_p = \alpha + \beta \times Z_p + \epsilon_p, \text{with } \epsilon_p \sim \mathcal{N}(0, \sigma^2). \tag{5}$$

$Parome_p$ is the seasonal precipitations in mm for the pixel p, α is the y-intercept in mm, β is the slope expressed in mm/m, and Z_p is the altitude in m of the pixel p. The regression fit is performed using the maximum likelihood method implemented in the ® function *lm*. PLRs are derived from β using the following formula:

$$PLR = 100 \times 100 \times \frac{\beta}{\bar{P}}. \tag{6}$$

where $\bar{P}$ is the average seasonal precipitation from AROME over the area where the linear regression is performed. The slope of the regression β is multiplied by 100 twice, first to obtain the result as a percentage and once more to express PLR in percentage per hundred meters (%/100 m), relative to the average seasonal precipitation from AROME. The expression of PLR in %/100 m overcomes the biased nature of gridded precipitation products and allows a spatial comparison despite significant spatial and seasonal variation in precipitation amounts across France (Fig.2). To investigate the dependence of PLR on a given spatial scale, regressions will be conducted on 23 massifs of the Alps and catchments. On the catchments, a regression will only be performed if there is sufficient variability in elevation, *i.e.* if the standard deviation of altitude is higher than 50 m.

3.3 Linearity of the regressions

In our formulation (Eq. 6), PLRs are defined as the slopes of the linear regressions. The linearity of the relationship between annual precipitation and altitude at the catchment scale is a questionable hypothesis. For example, Avanzi et al. (2021) found non-linearity in two catchments located in the Italian Alps. Smoothing splines provide more flexibility than linear regressions to model annual precipitation through altitude. However, smoothing splines are not interpretable in terms of PLRs. For this reason, we use piecewise linear regressions implemented in the ®️ package *segmented* (Muggeo, 2008). We perform piecewise linear regressions (unknown break-point between the first and third quartile of altitude) between annual precipitation and altitude on all catchments with sufficient variability (standard deviation of the altitude higher than 50 m) in altitude. To compare the linear (M_0 model) and the piecewise (M_1 model) linear models, taking inspiration from the Bayes factor defined in the Bayesian paradigm (Kass and Raftery, 1995), we compute the logarithm of the BIC ratio (B_r) as:

$$B_r = \frac{BIC_{M_0} - BIC_{M_1}}{2} \tag{7}$$

If the logarithm of B_r equals zero, the two models fit the data with the same quality. Negative values indicate better fits and positive values refer to worse fits than the linear regression.

B_r category (log scale)	Interpretation
<0	Anecdotal evidence for M_0
0 to 4.5	Anecdotal evidence for M_1
4.5 to 9	Moderate evidence for M_1
9 to 13.5	Strong evidence for M_1
>13.5	Decisive evidence for M_1

Table 2. Interpretation of the chosen categories of B_r. M_0 refers to the linear model and M_1 to the piecewise linear model.

4 Results

4.1 Ability of gridded precipitation products to reproduce the variability of the relationship between annual/seasonal precipitations and elevation

The altitude dependencies of the gridded precipitation products are compared to those from rain gauge data in the regions presented in Fig. 1(**a**). Figure 3(**a**) displays the median annual precipitation by 300 m altitudinal bands, for the seven gridded precipitation products, extracted at the location of the stations. In all regions of interest, annual precipitation observed at stations (*i.e.* the black curves showing the annual precipitations obtained with the rain gauges and NPT) increases as a function of the altitude. In the mid-range mountains such as the Northern Massif Central, the Southern Massif Central, and the foothills of the Alps, the annual precipitation always increases from one altitudinal band to another. The maximum increase of observed annual precipitation occurs in the foothills of the Alps with a gain of 500 mm in 1500 m altitude. In more complex topographical regions such as the Northern Alps, the Southern Alps, and the Pyrénées, the enhancement of annual precipitation with the

altitude is unclear, and only visible on a reduced range of altitude. For instance, the observed annual precipitation does not seem to increase in the Pyrénées below 1800 m. In mountain regions, even the mid-range ones like the foothills of the Alps, ERA5-Land, PDIR, and SERVAL often lead to more moderate increases in annual precipitation with the altitude compared

315 to the stations. In the Cévennes/Causses region, annual precipitation from ERA5-Land slowly changes with altitude. In the Northern Massif Central, all gridded precipitation products, except for PDIR, are in agreement with the observed enhancement of precipitation with altitude. In the foothills of the Alps, the underestimation of SERVAL increases through the altitudinal bands, reaching 1000 mm at 1500 m altitude. AROME overestimates annual precipitation in all regions of interest, and the bias generally increases at high altitudes. For example, at 2400–2700 m in the Southern Alps, AROME captures more than 1500

320 mm of median annual precipitation, while the stations record only 1000 mm. Nevertheless, median annual precipitation from AROME and observations are strongly correlated. Without data assimilation, AROME reproduces abrupt rises in precipitation at high altitudes. In the Northern Alps, AROME and the observed precipitations increase by the same amount of 500 mm from 1800–2100 m to 2100–2400 m. In some regions of interest such as the Pyrénées and the Northern Massif Central, the bias of AROME is constant through the altitudinal bands. It reflects that, in those regions, the altitude impacts AROME and the

325 station precipitations in the same way. The reanalysis CERRA-Land, based on rain gauges, is biased in some regions (Cévennes/Causses, Northern Alps, Pyrénées, Southern Massif Central). The bias is not constant and can be positive at low altitudes and negative at high altitudes such as in the Pyrénées region. The bias of CERRA-Land is relatively small in comparison to the bias of ERA5-Land, PDIR, SERVAL, and AROME as it reaches a maximum of 375 mm in the Northern Alps at 1800–2100 m. The reanalysis COMEPHORE and the interpolator SPAZM accurately reproduce precipitation data from stations in all regions

330 of interest, as both products assimilate rain gauge values. However, COMEPHORE underestimates precipitation above 2100 m, which is only visible in high-altitude regions, such as the Northern Alps and the Southern Alps. In the Northern Alps, the median annual precipitation from COMEPHORE is smaller than 1000 mm at 2400–2700 m, compared to more than 1300 mm measured with stations for the same altitudinal band. Figure 3(**a**) shows that COMEPHORE, CERRA-Land, and SPAZM reproduce well the relationship between altitude and observed annual precipitation in the regions of interest. AROME, with-

335 out rain gauge assimilation, exhibits the same precipitation/altitude trends that the stations, although it usually overestimates annual precipitation, especially at high altitudes. It can be added that the relationship between annual precipitation and altitude derived from the location of stations is dependent on the spatial sampling, which explains the variability of the curves in Fig.3(**a**). Nevertheless, the poor relationships between the annual precipitation obtained with ERA5-Land, PDIR, and SERVAL and the altitude disqualify them for further analysis of the PRLs.

340   Figure 3(**b**) shows the median precipitations by altitudinal bands on a seasonal basis, at station locations (solid curves), and by considering all the pixels belonging to a region (dotted curves). The study of seasonal precipitations is extended above the altitude of the stations. The results are only displayed for the four highest altitude regions (Foothills of the Alps, Northern Alps, Pyrénées, Southern Alps). Only precipitation from AROME, CERRA-Land, COMEPHORE, and SPAZM are investigated seasonally because of the highly biased nature of annual precipitation from ERA5-Land, PDIR, and SERVAL. Figure S2 in

345 the Supplement presents the results for all seasons, products, and regions. At station locations (solid curves), the seasonal precipitations from AROME, CERRA-Land, COMEPHORE, and SPAZM are close to the observed ones. Only AROME

overestimates seasonal precipitations, but the bias is not altitude-related. The relationship between seasonal precipitations and altitude is different at station locations (solid curves) and with all pixels (dotted curves) in the Northern and Southern Alps. The dotted curves are more regular and above the solid ones, illustrating that the stations are not representative of the altitudinal bands of the regions. When all pixels belonging to a region (dotted curves) are taken into account, differences grow among seasonal precipitations from AROME, CERRA-Land, COMEPHORE, and SPAZM. COMEPHORE experiences both lower winter and summer precipitation than AROME, CERRA-Land, and SPAZM. COMEPHORE precipitation remains unchanged or even decreases with altitude. As a result, the differences in precipitation amounts between COMEPHORE and the other products become larger in high altitudes. For example, in the Northern Alps, the winter precipitations from AROME, CERRA-Land, and SPAZM increase by 250 mm between 3000–3300 m to 3300–3600 m whereas COMEPHORE declines between these two altitudinal bands, leading to a 350 mm gap. CERRA-Land and SPAZM show common seasonal precipitation patterns with altitude in the Northern Alps and the Pyrénées. In the Northern Alps, CERRA-Land and SPAZM agree on slow changes in seasonal precipitations below 3000 m and more rapid increases above this threshold. In the Southern Alps, the increase of seasonal precipitations with altitude is larger with SPAZM than CERRA-Land. AROME produces a larger amount of seasonal precipitations in comparison to COMEPHORE, CERRA-Land, and SPAZM, especially in winter. In summer, AROME shows a suspicious precipitation amount of 1500 mm at high altitudes in the Northern Alps. In winter, the difference between AROME and the other gridded products is larger at high altitudes. For instance, in the foothills of the Alps, AROME matches SPAZM producing 250 mm at 0–300 m but is 300 mm higher at 2400–2700 m.

To investigate the ability of AROME, CERRA-Land, COMEPHORE, and SPAZM to reproduce the observed precipitation change with altitude at a fine spatial scale, Fig. 4 shows scatter plots of observed versus gridded precipitation relative difference (PRD). PRDs are defined for two neighboring (closest) stations as the difference in precipitation relative to the difference in altitude, see Sect. 3.2. PRDs are computed on all pairs of closest stations within the region of interest. Fig. S3 in the Supplement presents the PRDs scatter plots for all seasons. The same results observed in Fig. 3(**b**) appear. PRDs from COMEPHORE and SPAZM are unbiased, the points being close to the 1:1 lines. The variance of PRD errors is higher with AROME and CERRA-Land. PRDs from CERRA-Land seem unbiased on average, and those from AROME are a little too high in winter. Fig. 4 also reveals more difficulties for AROME, CERRA-Land, COMEPHORE, and SPAZM to reproduce observed summer than winter PRDs. PRDs with AROME are unbiased on average. This is possible to use AROME to model the altitude effect on seasonal precipitations at a fine spatial scale.

Figure 5 illustrates the relationship between seasonal precipitations and elevation through two transects in the Cévennes and the Northern Alps. A transect indicates a virtual line crossing the topography. Figure S4 in the Supplements shows the transects for all seasons. Seasonal precipitations from SPAZM are, by construction, fully correlated to the altitude, reacting to slight variations of terrain. COMEPHORE and CERRA-Land are both less correlated to the altitude than SPAZM. CERRA-Land gives the same winter precipitation as SPAZM but different summer precipitation patterns. COMEPHORE produces similar amounts of precipitation as SPAZM in the Cévennes transect but lower ones in the Northern Alps transect. AROME has a strong relationship with the altitude. It is the gridded product with usually the highest seasonal amounts in high altitudes.

For example, winter precipitations reach 600 mm in the Cévennes with AROME, almost 500 mm with SPAZM, and 400 mm with COMEPHORE and CERRA-Land.

COMEPHORE and CERRA-Land sometimes exhibit a negative correlation to the altitude. The behavior of COMEPHORE is surprising in the Northern Alps between 8 and 15 km after the beginning of the transect. COMEPHORE summer precipitation amount is the lowest for the highest pixel on the transect. CERRA-Land is different from the other gridded products in summer on the Cévennes with a negative association with the altitude for the first 80 km of the transect. SPAZM exhibits a higher correlation than AROME to the local topography. As a result, SPAZM precipitation maximums coincide with the summits while those of AROME are reached before the summits in the Northern Alps, for example. Another major difference between AROME and SPAZM is the seasonality of precipitation. In the first 20 km of the Northern Alps transect, while SPAZM shows similar seasonal precipitation patterns, AROME seasonality is more marked with two peaks in precipitation in winter at 5 and 15 km and only one in summer. Moreover, in the Northern Alps transect, SPAZM produces higher summer precipitation than winter precipitation (400 mm against 300 mm), unlike AROME.

Overall, AROME and SPAZM demonstrate the ability to replicate the altitude-dependent variations of annual and seasonal precipitations in the regions of interest. In comparison to commonly used gridded precipitation products such as satellite and radar data, AROME and SPAZM exhibit stronger correlations with observed precipitation. The evolution of AROME seasonal precipitations with altitude is consistent with that of stations, despite suspicious summer precipitation in very high altitudes in the Northern Alps and a too rapid rise of winter precipitation. In regions with sparse networks of stations, products based on stations such as SPAZM may be unable to capture the impact of local topography on precipitation. Since our objective is to investigate the spatial variability of PLR at the catchment scale, SPAZM will be inadequate for this purpose. AROME should be preferred to SPAZM in ungauged areas. PLRs are therefore computed with AROME simulations from 1982 to 2018. The long temporal period of more than 30 years allows for the investigation of PLR at the climatological scale.

4.2 Spatial and seasonal variability of Precipitation Lapse Rates

Initially, seasonal PLRs are computed at the sub-regional scale on the 23 massifs in the French Alps. Secondly, seasonal PLRs are computed on catchments that form a subdivision of the massifs. Figure 6(**a**) displays the R^2 at the sub-regional (massif) scale of the regressions between AROME seasonal precipitations and the altitude. Values of PLRs and R^2 at the sub-regional scale are provided in Table 4. In winter, values of R^2 are close to 0.5 in the foothills of the Alps (Chartreuse, Bauges, Aravis, Chablais), in the Northern Alps (Beaufortin, Belledonne, Mont-Blanc), and in the Southern Alps (Queyras, Thabor, Oisans, Devoluy, Champseur, Pelvoux, Ubaye, Haut-Var-Haut-Verdon). Regression quality in the Central Alps (Grandes-Rousses, Maurienne, Vanoise, Haute-Tarentaise) is not high enough to conclude on PLR values. Winter precipitation from AROME is for instance not correlated to the altitude in the Haute-Tarentaise massif (R^2 equals 0.12). In summer, the same spatial pattern is observed with lower values of R^2, indicating that the altitude is better correlated with winter precipitations than summer precipitations in the French Alps.

The fine resolution of AROME provides the possibility to investigate the spatial variability of the relationship between seasonal precipitations and altitude at the catchment scale. Figure 6(**c**) shows the R^2 values at the catchment scale. R^2 obtained

from regressions are higher at the catchment scale than at the sub-regional scale for both winter and summer seasons. Similarly to the sub-regional scale, R^2s are generally higher in winter than in summer. In winter, regression quality does not show a clear spatial pattern except for lower R^2 in the Eastern Alps (Haute-Tarentaise, Haute-Maurienne, Thabor, Queyras). The R^2s show a large spatial variability. In the foothills of the Alps (Vercors, Chartreuse, Bauges, Aravis), strong R^2 (0.75–1) can be found at the borders of the massifs next to small R^2 (0–0.5) inside the massifs. In summer, the regressions are of poor quality in the Northern and Central Alps. The massifs in the Southern Alps and some in the foothills of the Alps (Chartreuse, Bauges, Chablais) do not show a clear deterioration of R^2 compared to the winter. In some massifs like the Maurienne, in winter, the R^2 are superior to 0.5 at the catchment scale and close to 0 at the sub-regional scale. In the same way, the massifs, where the regression fits are correct at the sub-regional scale (Thabor, Haute-Maurienne), do not necessarily contain the best fit at the catchment scale. It indicates that the previous regressions (Fig.6**(a)**) are likely conducted over excessively broad areas.

Figures 6**(b),(d)** respectively display the PLRs of AROME seasonal precipitations at the sub-regional and catchment scales. We remark higher PLRs at the catchment scale (a mean of 5.43 %/100 m in winter and 3.31 %/100 m in summer) than at the sub-regional scale (a mean of 4.73 %/100 m in winter and 2.79 %/100 m in summer). We consider that a R^2 inferior to 0.5 is too small to interpret the slope of the regressions. The spatial variability of seasonal PLRs can therefore not be investigated at the sub-regional scale. We will only describe PLR values at the catchment scale because of better regressions. Figure 6**(d)** reveals higher PLRs in winter with very high values (8-15 %/100 m) and high values (5-8 %/100 m) mainly located at the border of the Alps (Devoluy, Thabor, Chablais). Moderate (3-5 %/100 m) PLRs are present in almost all massifs and do not show a clear spatial pattern, such as a North-South separation. Small (0-3 %/100 m) PLRs are mainly found inside the massifs of the foothills of the Alps (Vercors, Chartreuse, Aravis) and in the Far-Southern Alps (Mercantour, Haut-Var-Haut-Verdon). In summer, the majority of PLRs are small (0-3 %/100 m), but some catchments at the border of the Alps (Bauges, Devoluy, Haut-Var-Haut-Verdon) have moderate (3-5 %/100 m) or high PLRs (5-8 %/100 m). Figure 6 shows that the quality and slope of the regression can vary widely across the French Alps, with higher values at the borders. A sub-region like the Vercors massif covers around 1,350 km^2 and presents a considerable geographic heterogeneity in PLR values. Figures S5, S6, S7, and S8 in the Supplements illustrate the results of the regressions for all seasons.

Figure 7 shows the winter and summer PLRs at the catchment scale in the study domain. Results for the other seasons are available in Fig. S9 and S10 in the Supplements. The catchments located in the Morvan, the Massif Central, the Jura, the Eastern Pyrénées, and the catchments close to the Mediterranean with enough altitude variation (standard deviation of the altitude higher than 50 m) have the strongest PLRs. These values are higher than those of the Alps, as they can reach 32 %/100 m. Values between 8 and 15 %/100 m are also considerably more frequent than in the Alps. In the study domain, 40 % of the catchments with $R^2 > 0.5$ have winter PLR greater than 8 %/100 m. This percentage drops to 15 % if we only consider the Alps. The slopes of the regression have higher variability in the Alps and the Pyrénées. PLRs are seasonally varying, with generally the highest values in winter. In winter, the Massif Central hosts the strongest PLRs. In summer, the Mediterranean area, ranging from the Eastern Pyrénées to the Mediterranean Alps, has the highest PLRs.

To summarise, PLRs are generally higher in winter than in summer. PLRs are sensitive to the spatial scale, with higher values at the catchment scale than the sub-regional (massif) scale. Spatial patterns of significant PLRs vary according to the

Massif Number	Massif Name	DJF PLR (% /100 m)	JJA PLR (% /100 m)	DJF R^2	JJA R^2
1	Chablais	5.9	2.7	0.57	0.45
2	Aravis	4.3	2.3	0.45	0.43
3	Mont-Blanc	4.1	4.3	0.66	0.45
4	Bauges	4	3.6	0.5	0.52
5	Beaufortin	4.1	1.9	0.45	0.21
6	Haute-Tarentaise	2.2	0	0.11	0
7	Chartreuse	5.4	3.9	0.57	0.58
8	Belledonne	6.6	4.1	0.8	0.66
9	Maurienne	2.1	0.3	0.11	0
10	Vanoise	3.5	0.6	0.31	0.01
11	Haute-Maurienne	5.2	3.5	0.51	0.39
12	Grandes-Rousses	3.6	1.3	0.28	0.09
13	Thabor	9.1	5.2	0.52	0.34
14	Vercors	4.5	1.7	0.31	0.14
15	Oisans	4	1.4	0.55	0.21
16	Pelvoux	6.3	4.3	0.49	0.52
17	Queyras	5.5	4.2	0.51	0.49
18	Devoluy	6.8	3.5	0.56	0.3
19	Champsaur	4.7	3	0.67	0.58
20	Parpaillon	2.8	3.2	0.17	0.5
21	Ubaye	4.3	2.2	0.48	0.46
22	Haut-Var-Haut-Verdon	3.2	2.3	0.49	0.36
23	Mercantour	2.6	2.9	0.28	0.33

Table 3. Values of precipitation lapse rates (precipitation change per 100 m altitude difference divided by area-averaged precipitation) and R^2 at the sub-regional scale for the 23 French massifs for both winter *DJF* and summer *JJA*. The Massif Number is indicated in Fig. 6.

season in France. In winter, the higher PLRs reach 32 %/100 m and are mainly located in the Massif Central. In summer, PLRs are lower and reach larger values on the Mediterranean coast. PLRs vary notably in space, even within a single mountain range such as the French Alps.

4.3 Linearity of the relationship between annual precipitation and altitude

To assess the linearity of the regressions performed in Fig. 7, piecewise linear regressions were compared to linear regressions through BIC ratio (see subsection 3.3). Figure 8(**a**) illustrates the BIC ratio categories (Table 2) with some examples of scatter plots and corresponding regressions. Colors refer to categories of the logarithm of B_r. Based on the scatter plots, we consider the relationship between annual precipitation and altitude not linear when there is strong or decisive evidence for M_1 (red color). Figure 8(**b**) shows the spatial distribution of the logarithm of the B_r values. 10 % of the catchments show decisive evidence for M_1. It appears mainly in the Massif Central, the Jura, and the Southern Alps. In the other regions (Northern Alps, Pyrénées), it is sufficient to use linear regression to derive PLR. Figure 8(**c**) shows the distribution in surface areas of the catchments among the five categories of B_r. Strong B_r are mainly found for large catchments, revealing the spatial scale dependence of PLR discussed in subsection 5.3. Too much spatial heterogeneity is still present in some catchments (last scatter plot in Fig. 8(**a**)), suggesting an even finer spatial division, taking into account the aspect and the slope of the terrain faces.

Large catchments can have slopes with different orientations for instance. Figure S12 in the Supplements provides the same diagnostic of linearity for AROME seasonal precipitations.

In 90 % of the catchments, the regression between seasonal precipitation and altitude can be considered linear. The remaining 10 % often corresponds to larger catchments, which could motivate the estimation of the PLRs on smaller areas in these cases.

5 Discussion

5.1 Ability of gridded precipitation products to capture the relationship between annual/seasonal precipitations and altitude

This article reviews the potential of seven gridded precipitation products for precipitation gradient estimation in a complex topographic region. ERA5-Land, PDIR, and SERVAL underestimate annual precipitation gradients even for mid-range mountains. The limitations of these three gridded precipitation products are even more apparent in high-altitude regions such as the Northern Alps and the Southern Alps. The assimilation of satellite data and the non-use of rain gauge values in ERA5-Land and PDIR is an obstacle to their utilization in a complex topographic region such as France. These findings converge with those of Jiang et al. (2022), where they found that the satellite product IMREG cannot reproduce the precipitation gradient in Tibet. SERVAL does not use altitude as a co-variable to determine precipitation from individual radars. The uniform ratio applied for this product in the hourly correction only represents the station elevation range, not the entire radar coverage. The translation of reflectivity to precipitation amount using the vertical profile of reflectivity is another potential source of error that results in inaccurate negative precipitation gradients in Fig.3. In their study of the French Alps at the sub-regional level, Faure et al. (2019) found a significant underestimation of precipitation gradient using PANTHERE, SERVAL's predecessor.

CERRA-Land, COMEPHORE, and SPAZM assimilate ground precipitation measurements from weather stations and are thus correlated with the annual precipitation observed at the stations. COMEPHORE leads to an adequate relationship between annual/seasonal precipitations and altitude in mid-mountain ranges highly instrumented as the Southern Massif Central. However, in more complex topographical regions with sparse stations such as the Northern Alps, COMEPHORE relies heavily on radar data from high altitudes and is unable to accurately reproduce the increase of precipitation with altitude. COMEPHORE processes fewer high-altitude stations than SPAZM, making it unable to represent precipitation in high-altitude areas correctly. The sharp decrease of summer precipitation with altitude from COMEPHORE in the Northern Alps illustrated in Fig.5(**d**) is likely due to the shielding of the radar beams by mountain ranges (Germann et al., 2006). CERRA-Land can replicate the observed seasonal precipitation enhancement with the altitude. However, at the annual scale, CERRA-Land is slightly biased in some regions, and the bias may change of sign according to altitudinal bands such as in the Pyrénées (Fig.3(**a**)). SPAZM can reproduce the relationship between annual precipitation at station locations and altitude at the regional scale. This result is not surprising as SPAZM interpolates precipitation observations from the stations, incorporating the effect of the altitude through local linear regressions. However, SPAZM is affected by the density of stations. In regions where the stations are more sparse, as in the Pyrénées, annual precipitations from SPAZM do not match annual precipitations from the stations. This suggests a possible limitation of SPAZM in ungauged mountainous regions. AROME, without rain gauge assimilation, can reproduce

the relationship between seasonal precipitations and altitude, despite a positive bias in winter in mountainous regions. We find that AROME produces higher annual/seasonal precipitations than the other gridded products. The difference in seasonal precipitations is limited at low altitudes and rises sharply at high altitudes. Higher precipitation accumulations with RCMs have been documented. In Western Montana, in high-altitude where observations are sparse, Silverman et al. (2013) remarked higher annual precipitation with the Weather Research and Forecasting (WRF) model than with the Parameter-elevation Regressions on Independent Slopes Model (PRISM) (Daly et al., 1994). In India, Li et al. (2017) found that annual precipitations obtained with WRF are twice or triple the amount of the satellite precipitation product Tropical Rainfall Measuring Mission (TRMM). The correlation between AROME and COMEPHORE on the Cévennes transect in summer (Fig.5(**c**)) is comforting as the radars operate well in summer in the Cévennes region (Delrieu et al., 2013). Moreover, the seasonality of precipitation is taken into account with AROME (see Fig.5(**c**)). AROME simulates precipitation without using rain gauge data ~~. As a result, precipitation under-catch in~~ and poorly matches the high-elevation ~~stations does not affect AROME simulations. Precipitation under-catch is more common in winter . This partly explains the precipitation difference~~ gauges, which could be the combined effect of precipitation undercatch (Groisman and Legates, 1994; Sevruk, 1997; Pollock et al., 2018) and some deficiencies in AROME (Monteiro et al., 2022). In Fig. 3(**b**), AROME shows a strong agreement with the rain gauges in summer, even the high-altitude ones. The differences are larger in winter, where precipitations mostly fall as snow. Precipitation undercatch is limited in summer and more important in winter with solid precipitation. This suggests that precipitation undercatch could partly explain the differences between AROME and ~~the other products in winter and the agreement in summer in Fig. 3.~~ rain gauges.

To summarize, this study shows that the simulations of the CP-RCM AROME, despite winter precipitation overestimation, offer the opportunity to derive PLRs at a fine spatial scale. The other grid precipitation products obtained from radar, satellite, or rain gauge data show important limitations in a complex topography region. Radar is among others subjected to beam blocking. Satellite resolution is too coarse to represent the altitude effect on precipitation. Rain gauge networks are too sparse and even high-density ones do not account for the spatial and altitudinal variability of seasonal precipitation.

5.2 Values and spatial variability of Precipitation Lapse Rates

Table 4 synthesizes the main research on PLRs. Like Ménégoz et al. (2020) in Switzerland, we find higher PLRs in winter, likely due to the large-scale circulation of air masses. In winter, the Western wind coming from the Atlantic loaded with moisture is dominant and hits the primary mountainous regions on its way. The affected catchments correspond to the first orographical barrier and are located in the Massif Central, extending from the Languedoc to the Morvan regions. On those catchments, 50 % of the PLRs are in the range of 5–13 %/100 m. For the same reason, the PLRs are in the range of 5–15 %/100 for the first Western catchments of the Alps. Interestingly, a distinct pattern emerges in the Thabor where some PLRs are in the range of 8–15 %/100 m due to frequent Easterly weather fronts brought by Mediterranean circulation from Italy. In summer, the Mediterranean area is subjected to the dominant Southern flows and hosts the highest PLRs. The Southern air masses absorb the humidity from the Mediterranean Sea. For this reason, we found higher PLRs in the Eastern Pyrénées (8–15 %/100 m) compared to the Central Pyrénées (3–8 %/100 m). Convective processes are more frequent in summer than in

winter. Daily precipitation amounts from convective processes are often negatively correlated to the altitude (Schäppi, 2013). That is likely to explain the lower PLRs in summer than in winter. To summarise, we notice high PLRs in areas subjected to the prevailing winds in France, which are Western, Southern, and Eastern winds depending on the season. Like Kotlarski et al. (2012), we find lower PLRs in the Alps than in the rest of France.

535   In the French Alps, a complex topographical region, we do not find a significant difference in PLR values between the Northern and the Southern Alps for the winter and summer seasons contrary to Sevruk (1997); Durand et al. (2009); Ménégoz et al. (2020). That is probably due to the finer spatial scale used in the study. At a larger spatial scale, large-scale circulation, rather than the local topography, drives seasonal precipitation amounts (Jiang et al., 2022). We find a large spatial variability of PLRs, which can vary inside the same massif from one catchment to another. For instance, winter PLRs range from 3–5

540   %/100 m to 8–15 %/100 m in Belledonne. Using rain gauges, Ogrin and Kozamernik (2018) highlighted the extreme spatial variability of PLRs in the range of 5–16 %/100 m for the summer season in three nearby alpine valleys of Slovenia. We find the same magnitude in PLR values and variability. PLRs are highly spatially varying in high-altitude and complex topographical regions such as the French Alps and Pyrénées. In the Massif Central, PLRs exhibit less spatial variability.

Study domain	Data	Spatial scale	Period	Findings	Reference
Switzerland	Rain gauges	massifs 4,000 km^2	1951–1980	Northern Alps: 5.4 %/100 m Southern Alps: 0.24 %/100 m	Sevruk (1997)
French Alps	SAFRAN	regions 1,000–10,000 km^2	1958–2002	Northern Alps: 29.4 mm/100 m Central Alps: 19.5 mm/100 m Southern Alps: 17.2 mm/100 m Mediterranean Alps : 17.8 mm/100 m	Durand et al. (2009)
Europe	RCM	country 200,000–1,000,000 km^2	1961–2000	Spain: -3.7 mm/100 m United-Kingdom: 131 mm/100 m France (without the Alps and the Pyrénées): 32 mm/100 m Alps: 14.6 mm/100 m	Kotlarski et al. (2012)
Slovenia	Rain gauges		2012–2015 (MJJASON)	5–16 %/100 m	Ogrin and Kozamernik (2018)
Swiss and French Alps	RCM	regions 10,000–50,000 km^2	1971–2008	French Northern Alps: 2.6 %/100 m French Southern Alps: 1.6 %/100 m Swiss Alps: 4.3 %/100 m in winter (DJF) 2 %/100 m in summer (JJA)	Ménégoz et al. (2020)
Third pole	WRF	regions (1,000,000 km^2) catchments (10,000 km^2)	1980-2018	regions: 2.90–11.26 %/100 m Large catchments: -10–10 %/100 m Small catchments: -4–10 %/100 m	Jiang et al. (2022)

Table 4. Summary of the studies on precipitation lapse rates (PLRs), namely study domain, data, spatial scale, period, findings, and reference.

In summary, PLRs are probably higher in winter because of the omnipresence of stratiform events that cause structured

545   orographic precipitation in catchments exposed to oceanic weather patterns. In summer, the air masses are coming from the Mediterranean Sea, causing high PLRs in the coastal and hilly Mediterranean areas. In this season, precipitation is mainly caused by the combination of multiple convective events, resulting in unclear PLR spatial patterns.

5.3   Dependence of the Precipitation Lapse Rates to the spatial scale

The low R^2 found in Fig.6**(a)** is a reminder of the high intra-massif variability of the relationship between seasonal precipitations and altitude in large sub-regions. The sub-regions dissection into more homogeneous areas, such as small catchments with a surface area close to 100 km^2 allows a better description of PLRs. Regressions at the catchment scale have larger PLR and R^2 values than at the sub-regional scale. In winter in Maurienne, all catchments have R^2 greater than 0.5 with PLRs in the range 3–8 %/100 m. The R^2 is close to 0, and the slope is close to 2 %/100 m with a single regression covering all the Maurienne massif. Figure 9 shows the scatter plot between AROME annual precipitation and altitude for the pixels within three groups of catchments in the Vercors, a massif covering 1,350 km^2. The colors of pixels relate to distinct geographical locations. Figure S11 in the Supplements provides the scatter plots for seasonal precipitations. Figure 9 suggests that the Vercors encompasses several sub-regions with different relationships between annual precipitation and altitude. This relationship is linear for the Southern and Western Vercors catchments. However, the Western and Southern Vercors are not subject to the same meteorological influences. The PLRs are higher in the Western Vercors because of the dominant rainy westerly flow. The relationship is not linear for the catchments located in the Vercors plateaus. The attenuation of orographic precipitation after crossing the first hills of the West of the massif is a possible explanation. Figure 9 reveals the coexistence of PLR spatial patterns within a single massif.

In the French Alps, a complex topographical region, it is not appropriate to calculate PLRs on too vast sub-regions with surface areas of more than 1,000 km^2. In vast sub-regions, there is a risk of mixing areas with too much spatial heterogeneity and losing information about PLR spatial variability. Investigation of PLR with stations or stations-based precipitation products such as SPAZM should be conducted carefully in sparse station networks. For example, in the Aravis massif covering 1,070 km^2, linear regressions between precipitation and altitude in SPAZM are performed using all stations within the massif to ensure robustness. However, Fig. 6**(d)** indicates that the Aravis has high intra-massif variability of winter PLR with lower values in its western part. SPAZM can not capture this variability.

5.4   ~~Linearity of the relationship between annual precipitation and altitude~~

~~In our formulation (Eq. 6), PLRs are defined as the slopes of the linear regressions. The linearity of the relationship between annual precipitation and altitude~~ PLRs are thus scale-dependent. The linear regressions give better R^2 and larger PLRs at the catchment scale ~~is a questionable hypothesis. For example, Avanzi et al. (2021) found non-linearity in two catchments located in the Italian Alps. Smoothing splines provide more flexibility than linear regressions to model annual precipitation through altitude. However, smoothing splines are not interpretable in terms of PLRs. For this reason, we use piecewise linear regressions implemented in the package *segmented* (Muggeo, 2008). We perform piecewise linear regressions (unknown break-point between the first and third quartile of altitude) between annual precipitation and altitude on all catchments with sufficient variability (standard deviation of the altitude higher than 50 m) in altitude. To compare the linear (M_0 model) and the piecewise (M_1 model) linear models, taking inspiration from the Bayes factor defined in the Bayesian paradigm (Kass and Raftery, 1995)~~

580 , we compute the logarithm of the BIC ratio (B_r) as:

$$B_r = \frac{BIC_{M_0} - BIC_{M_1}}{2}$$

If the logarithm of B_r equals zero, the two models fit the data with the same quality. Negative values indicate better fits and positive values refer to worse fits than the linear regression. (100 km^2) than at the sub-regional scale (1,000 km^2). Too broad sub-regions often hide distinct altitude effects on precipitation.

585 B_r category (log scale)Interpretation <0 Anecdotal evidence for M_0 0 to 4.5 Anecdotal evidence for M_1 4.5 to 9 Moderate evidence for M_1 9 to 13.5 Strong evidence for M_1 >13.5 Decisive evidence for M_1 Interpretation of the chosen categories of B_r. M_0 refers to the linear model and M_1 to the piecewise linear model.

Figure 8(a) illustrates the BIC ratio categories (Table 2) with some examples of scatter plots and corresponding regressions. Colors refer to categories of the logarithm of B_r. Based on the scatter plots, we consider the relationship between annual
590 precipitationand altitude not linear when there is strong or decisive evidence for M_1 (red color). Figure 8(b) shows the spatial distribution of the logarithm of the B_r values. 10 % of the catchments show decisive evidence for M_1. It appears mainly in the Massif Central, the Jura, and the Southern Alps. In the other regions (Northern Alps, Pyrénées), it is sufficient to use linear regression to derive PLR. Figure 8(c) shows the distribution in surface areas of the catchments among the five categories of B_r. Strong B_r are mainly found for large catchments, revealing the spatial scale dependence of PLR discussed in subsection
595 5.3. Too much spatial heterogeneity is still present in some catchments (last scatter plot in Fig. 8(a)), suggesting an even finer spatial division, taking into account the aspect and the slope of the terrain faces. Large catchments can have slopes with different orientations for instance. Figure S12 in the Supplements provides the same diagnostic of linearity for AROME seasonal precipitations.

(a) Scatter plots of AROME annual precipitation (mm) as a function of the altitude for some catchments taken as illustrative
600 examples of the different categories of BIC ratio. Linear (red lines) and piecewise linear (blue curves) regressions are superimposed.
(b) Spatial representation of the logarithm of the BIC ratios between linear and piecewise linear regression (annual precipitation ~ altitude) models. The numbers expressed in % correspond to the percentage of catchments within the classes of the BIC ratio.
(c) Distribution of the surface area of the catchments according to the categories of BIC ratio.

5.4 Uncertainty in the study and outlooks

605 A limitation of our study is the potential undercatch of precipitation by the high-altitude stations. The underestimation can be as high as 50 % in winter during meteorological events with strong winds and a large proportion of snowfall. A 25 % underestimation of mountain annual precipitation is possible (Sevruk, 1997). In low altitudes, the underestimation is less severe. As a result, the comparison of PLRs in Fig.3(a) can lead to wrong conclusions on the bias of the gridded precipitation products. For the same magnitude of bias, our preference goes to seasonal precipitation overestimation rather than underestimation.
610 Despite the measuring uncertainty, we decided to include NPT in our study to account for high ungauged altitude regions. The available period from NPT differs from those of rain gauges and precipitation products. Additional data sources can enhance the spatial and altitudinal representation of PLR. High-altitude measurements of snow water equivalent (SWE) levels

can constrain the regressions between winter precipitation and altitude and make PLRs more robust. However, the transition from daily SWE to seasonal precipitations is highly temperature and snowmelt-dependent. For high altitude measurements, it is possible to make the strong assumption that only solid precipitation has occurred and that snowmelt has been minimal, as stated in Avanzi et al. (2021). Due to the high level of uncertainty of the measure, we opt not to include those data.

At high altitudes, winter precipitation from AROME is significantly higher than that of the other precipitation products, including SPAZM. At 2700–3000 ~~mp~~ m in the Pyrénées, AROME simulates an extra 400 mm of precipitation compared to COMEPHORE, CERRA-Land, and SPAZM. SPAZM may underestimate high-altitude precipitations due to precipitation under-catch. It is also likely that AROME overestimates seasonal precipitations. Indeed, Monteiro et al. (2022) found excessive snow accumulation with AROME in the French Alps above 1800 m. The authors advanced assumptions about spurious snow accumulation, such as the AROME cold temperature bias and the weakness of the AROME snowpack schemes. The winter PLR values given in Fig.7(b) for high-altitude catchments should be considered with precaution. In addition to AROME, various CP-RCMs listed in (Ban et al., 2021, Table1) have been used to simulate precipitation at a fine resolution in France. PLRs derived as the slope of linear regressions are necessarily uncertain because of the regression uncertainty. A perspective of the study could be to include prediction intervals, *i.e.* a range of values containing the "true" value with a probability of 0.95, for example.

6 Conclusion

We address the question of the spatial variability of seasonal precipitation lapse rates in France, a country with varied and complex topography. A dense rain gauge network enriched with snow rain gauge totalizators characterizes the relationship between annual/seasonal precipitations and altitude in large regions. The ability to reproduce this link obtained from ground measurements is analyzed using seven different kinds of gridded precipitation products: ERA5-Land, the PDIR satellite product, the raw radar product SERVAL, a 37-year simulation from the CP-RCM AROME, two reanalysis named CERRA-Land and COMEPHORE, and the precipitation interpolator SPAZM. Precipitation products commonly used in hydrology are limited in high-altitude regions with complex topography, such as the French Alps. Radar products perform well in hilly terrain but underestimate annual precipitation in high altitudes, resulting in a negative association between annual precipitation and altitude. Satellite products are not subject to the same estimation errors as radar products. However, the coarse resolutions do not accurately represent the annual precipitation altitude dependence in regions with topography heterogeneity. The performance of station-based products is dependent on the density of the weather station network. In ungauged mountainous areas, precipitation estimation from those kinds of products requires some degree of interpolation, whereas AROME uses physical laws. AROME does not incorporate rain gauge data and is therefore not subjected to bias caused by the under-sampling of particular high-altitude spatial areas. The simulations from the CP-RCM AROME, despite an overall overestimation of high-altitude precipitations, offer an opportunity to assess the altitude dependence of seasonal precipitations at the catchment scale. We employ the CP-RCM AROME to derive seasonal PLRs on 23 French Alps massifs and 2,748 catchments. The spatial-scale dependence of PLRs is investigated in the French Alps by comparing seasonal PLR values at the sub-regional (1,000 km^2) and

the catchment (100 km^2) scales. PLRs are derived using linear regression between seasonal precipitations and altitude. PLRs are spatial scale-dependent as they tend to be higher and better represented when computed at the catchment scale. The local topography influence on seasonal precipitations is major at a small spatial scale but dominated by the large-scale atmospheric circulation influence at the larger sub-regional spatial scale. PLRs are higher in winter. Winter PLRs are in the majority positive. 95 % of them are in the range 0.55–13.10 %/100 m. The higher values are found in the Westerly and Mediterranean dominant flow-exposed regions, reaching up to 32 %/100 m. In high-altitude regions such as the French Alps and the Pyrénées, we notice sheltering effects with PLRs close to 0 %/100 m for some catchments enclosed by mountains. It is generally the first reliefs encountered by air masses that host the stronger PLRs. This article emphasizes the importance of considering the topography on a fine spatial scale to estimate PLRs in ungauged mountainous regions. CP-RCM models offer an opportunity to compute the enhancement of seasonal precipitations with the altitude.

Code and data availability

SERVAL and COMEPHORE are available from the Aeris portal (https://radarsmf.aeris-data.fr/, last access: 21th December 2023). PDIR is available from the CHRS Data Portal (https://chrsdata.eng.uci.edu/, last access: 21th December 2023). ERA5-Land is available from Copernicus (https://cds.climate.copernicus.eu, last access: 21th December 2023). CERRA-Land is available from Copernicus (https://cds.climate.copernicus.eu, last access: 21th December 2023). AROME is available from the Med CORDEX Portal (https://www.medcordex.eu/search/index.php, last access: 21th December 2023). The spatial dataset containing the catchments is available from data.gouv (https://www.data.gouv.fr/fr/datasets/, last access: 21th December 2023). SPAZM and the stations are not available. The ® codes used to perform the analysis are available upon reasonable requests by directly contacting the first author.

Author contributions

GE and VD conceived the idea. VD carried out the analysis and wrote the article. GE, DP, and AF participated in the discussion and design of this study and contributed to writing and editing the paper.

Competing interests

The authors declare no conflict of interest.

Acknowledgements

We are grateful for the provision of AROME simulations by Cécile Caillaud and Diego Monteiro. This work benefits from the exchanges between the researchers of the CNRM (Centre National de Recherches Météorologiques) team of Meteo-France,

the researchers of IGE, and the engineers of EDF: special thanks to Martin Ménégoz and Samuel Morin that gave us pertinent comments. We also thank the three anonymous reviewers for their constructive feedback that improved the clarity of the article.

675 Financial support

This research has been supported by Electricité de France (EDF).

References

Avanzi, F., Ercolani, G., Gabellani, S., Cremonese, E., Pogliotti, P., Filippa, G., Morra Di Cella, U., Ratto, S., Stevenin, H., Cauduro, M., and Juglair, S.: Learning about precipitation lapse rates from snow course data improves water balance modeling, Hydrology and Earth System Sciences, 25, 2109–2131, https://doi.org/10.5194/hess-25-2109-2021, 2021.

Bales, R. C., Molotch, N. P., Painter, T. H., Dettinger, M. D., Rice, R., and Dozier, J.: Mountain hydrology of the western United States, Water Resources Research, 42, https://doi.org/10.1029/2005WR004387, _eprint: https://onlinelibrary.wiley.com/doi/pdf/10.1029/2005WR004387, 2006.

Ban, N., Caillaud, C., Coppola, E., Pichelli, E., Sobolowski, S., Adinolfi, M., Ahrens, B., Alias, A., Anders, I., Bastin, S., Belušić, D., Berthou, S., Brisson, E., Cardoso, R. M., Chan, S. C., Christensen, O. B., Fernández, J., Fita, L., Frisius, T., Gašparac, G., Giorgi, F., Goergen, K., Haugen, J. E., Hodnebrog, O., Kartsios, S., Katragkou, E., Kendon, E. J., Keuler, K., Lavin-Gullon, A., Lenderink, G., Leutwyler, D., Lorenz, T., Maraun, D., Mercogliano, P., Milovac, J., Panitz, H.-J., Raffa, M., Remedio, A. R., Schär, C., Soares, P. M. M., Srnec, L., Steensen, B. M., Stocchi, P., Tölle, M. H., Truhetz, H., Vergara-Temprado, J., de Vries, H., Warrach-Sagi, K., Wulfmeyer, V., and Zander, M. J.: The first multi-model ensemble of regional climate simulations at kilometer-scale resolution, part I: evaluation of precipitation, Climate Dynamics, 57, 275–302, https://doi.org/10.1007/s00382-021-05708-w, 2021.

Barrows: Precipitation and runoff and altitude relations for connecticut River, Eos, Transactions American Geophysical Union, https://agupubs.onlinelibrary.wiley.com/doi/abs/10.1029/TR014i001p00396, 1933.

Beck, J. and Bousquet, O.: Using Gap-Filling Radars in Mountainous Regions to Complement a National Radar Network: Improvements in Multiple-Doppler Wind Syntheses, Journal of Applied Meteorology and Climatology, 52, 1836–1850, https://doi.org/10.1175/JAMC-D-12-0187.1, publisher: American Meteorological Society Section: Journal of Applied Meteorology and Climatology, 2013.

Bell, B. A., Hughes, P. D., Fletcher, W. J., Cornelissen, H. L., Rhoujjati, A., Hanich, L., and Braithwaite, R. J.: Climate of the Marrakech High Atlas, Morocco: Temperature lapse rates and precipitation gradient from piedmont to summits, Arctic, Antarctic, and Alpine Research, 54, 78–95, https://doi.org/10.1080/15230430.2022.2046897, publisher: Taylor & Francis _eprint: https://doi.org/10.1080/15230430.2022.2046897, 2022.

Belušić, D., de Vries, H., Dobler, A., Landgren, O., Lind, P., Lindstedt, D., Pedersen, R. A., Sánchez-Perrino, J. C., Toivonen, E., van Ulft, B., Wang, F., Andrae, U., Batrak, Y., Kjellström, E., Lenderink, G., Nikulin, G., Pietikäinen, J.-P., Rodríguez-Camino, E., Samuelsson, P., van Meijgaard, E., and Wu, M.: HCLIM38: a flexible regional climate model applicable for different climate zones from coarse to convection-permitting scales, Geoscientific Model Development, 13, 1311–1333, https://doi.org/10.5194/gmd-13-1311-2020, publisher: Copernicus GmbH, 2020.

Bergström, S.: The HBV model–its structure and applications, SMHI, 1992.

Berne, A. and Krajewski, W. F.: Radar for hydrology: Unfulfilled promise or unrecognized potential?, Advances in Water Resources, 51, 357–366, https://doi.org/10.1016/j.advwatres.2012.05.005, 2013.

Brousseau, P., Seity, Y., Ricard, D., and Léger, J.: Improvement of the forecast of convective activity from the AROME-France system, Royal Meteorological Society, https://rmets.onlinelibrary.wiley.com/doi/abs/10.1002/qj.2822, 2016.

Buzzi, A., Tartaglione, N., and Malguzzi, P.: Numerical Simulations of the 1994 Piedmont Flood: Role of Orography and Moist Processes, Monthly Weather Review, 126, 2369–2383, https://doi.org/10.1175/1520-0493(1998)126<2369:NSOTPF>2.0.CO;2, publisher: American Meteorological Society Section: Monthly Weather Review, 1998.

Caillaud, C., Somot, S., Alias, A., Bernard-Bouissières, I., Fumière, Q., Laurantin, O., Seity, Y., and Ducrocq, V.: Modelling Mediterranean heavy precipitation events at climate scale: an object-oriented evaluation of the CNRM-AROME convection-permitting regional climate model, Climate Dynamics, 56, 1717–1752, https://doi.org/10.1007/s00382-020-05558-y, 2021.

Caine, N.: The rainfall intensity-duration control of shallow landslides and debris flows, Geografiska annaler: series A, physical geography, 62, 23–27, 1980.

Caracena, F., Maddox, R. A., Hoxit, L. R., and Chappell, C. F.: Mesoanalysis of the Big Thompson storm, Monthly Weather Review, 107, 1–17, 1979.

Champeaux, J.-L., Dupuy, P., Laurantin, O., Soulan, I., Tabary, P., and Soubeyroux, J.-M.: Les mesures de précipitations et l'estimation des lames d'eau à Météo-France : état de l'art et perspectives, La Houille Blanche, Numero 5, 28–34, https://doi.org/10.1051/lhb/2009052, 2009.

Conway, H. and Raymond, C.: Snow stability during rain, Journal of Glaciology, 39, 635–642, 1993.

Coppola, E., Sobolowski, S., Pichelli, E., Raffaele, F., Ahrens, B., Anders, I., Ban, N., Bastin, S., Belda, M., Belusic, D., Caldas-Alvarez, A., Cardoso, R. M., Davolio, S., Dobler, A., Fernandez, J., Fita, L., Fumiere, Q., Giorgi, F., Goergen, K., Güttler, I., Halenka, T., Heinzeller, D., Hodnebrog, O., Jacob, D., Kartsios, S., Katragkou, E., Kendon, E., Khodayar, S., Kunstmann, H., Knist, S., Lavín-Gullón, A., Lind, P., Lorenz, T., Maraun, D., Marelle, L., van Meijgaard, E., Milovac, J., Myhre, G., Panitz, H.-J., Piazza, M., Raffa, M., Raub, T., Rockel, B., Schär, C., Sieck, K., Soares, P. M. M., Somot, S., Srnec, L., Stocchi, P., Tölle, M. H., Truhetz, H., Vautard, R., de Vries, H., and Warrach-Sagi, K.: A first-of-its-kind multi-model convection permitting ensemble for investigating convective phenomena over Europe and the Mediterranean, Climate Dynamics, 55, 3–34, https://doi.org/10.1007/s00382-018-4521-8, 2020.

Cuo, L. and Zhang, Y.: Spatial patterns of wet season precipitation vertical gradients on the Tibetan Plateau and the surroundings, Scientific Reports, 7, 5057, https://doi.org/10.1038/s41598-017-05345-6, number: 1 Publisher: Nature Publishing Group, 2017.

Dallan, E., Marra, F., Fosser, G., Marani, M., Formetta, G., Schär, C., and Borga, M.: How well does a convection-permitting regional climate model represent the reverse orographic effect of extreme hourly precipitation?, Hydrology and Earth System Sciences, 27, 1133–1149, https://doi.org/10.5194/hess-27-1133-2023, 2023.

Daly, C., Neilson, R. P., and Phillips, D. L.: A Statistical-Topographic Model for Mapping Climatological Precipitation over Mountainous Terrain, Journal of Applied Meteorology and Climatology, 33, 140–158, https://doi.org/10.1175/1520-0450(1994)033<0140:ASTMFM>2.0.CO;2, publisher: American Meteorological Society Section: Journal of Applied Meteorology and Climatology, 1994.

Delrieu, G., Boudevillain, B., Wijbrans, A., Faure, D., Bonnifait, L., Kirstetter, P.-E., and Confoland, A.: Prototype de ré-analyses pluviométriques pour la région Cévennes-Vivarais, La Météorologie, 2013, 35–41, https://doi.org/10.4267/2042/52052, 2013.

Dozier, J., Bair, E. H., and Davis, R. E.: Estimating the spatial distribution of snow water equivalent in the world's mountains, WIREs Water, 3, 461–474, https://doi.org/10.1002/wat2.1140, _eprint: https://onlinelibrary.wiley.com/doi/pdf/10.1002/wat2.1140, 2016.

Durand, Y., Laternser, M., Giraud, G., Etchevers, P., Lesaffre, B., and Mérindol, L.: Reanalysis of 44 Yr of Climate in the French Alps (1958–2002): Methodology, Model Validation, Climatology, and Trends for Air Temperature and Precipitation, Journal of Applied Meteorology and Climatology, 48, 429–449, https://doi.org/10.1175/2008JAMC1808.1, publisher: American Meteorological Society Section: Journal of Applied Meteorology and Climatology, 2009.

Faure, D., Delrieu, G., and Gaussiat, N.: Impact of the Altitudinal Gradients of Precipitation on the Radar QPE Bias in the French Alps, Atmosphere, 10, 306, https://doi.org/10.3390/atmos10060306, number: 6 Publisher: Multidisciplinary Digital Publishing Institute, 2019.

750 Foley, A.: Uncertainty in regional climate modelling: A review, Progress in Physical Geography: Earth and Environment, 34, 647–670, https://doi.org/10.1177/0309133310375654, publisher: SAGE Publications Ltd, 2010.

Formetta: Differential orographic impact on sub-hourly, hourly, and daily extreme precipitation, Advances in Water Resources, https://doi.org/10.1016/j.advwatres.2021.104085, 2021.

Frei, C. and Isotta, F. A.: Ensemble Spatial Precipitation Analysis From Rain Gauge Data: Methodology and Application in the European

755 Alps, JGR Atmospheres, https://doi.org/10.1029/2018JD030004, 2019.

Garavaglia, F., Gailhard, J., Paquet, E., Lang, M., Garçon, R., and Bernardara, P.: Introducing a rainfall compound distribution model based on weather patterns sub-sampling, Hydrology and Earth System Sciences, 14, 951–964, https://doi.org/10.5194/hess-14-951-2010, publisher: Copernicus GmbH, 2010.

Garavaglia, F., Le Lay, M., Gottardi, F., Garçon, R., Gailhard, J., Paquet, E., and Mathevet, T.: Impact of model structure on flow simu-

760 lation and hydrological realism: from a lumped to a semi-distributed approach, Hydrology and Earth System Sciences, 21, 3937–3952, https://doi.org/10.5194/hess-21-3937-2017, publisher: Copernicus GmbH, 2017.

Gerber, F., Besic, N., Sharma, V., Mott, R., Daniels, M., Gabella, M., Berne, A., Germann, U., and Lehning, M.: Spatial variability in snow precipitation and accumulation in COSMO–WRF simulations and radar estimations over complex terrain, The Cryosphere, 12, 3137–3160, https://doi.org/10.5194/tc-12-3137-2018, publisher: Copernicus GmbH, 2018.

765 Germann, U., Galli, G., Boscacci, M., and Bolliger, M.: Radar precipitation measurement in a mountainous region, Quarterly Journal of the Royal Meteorological Society, 132, 1669–1692, https://doi.org/10.1256/qj.05.190, 2006.

Gomis-Cebolla, J., Rattayova, V., Salazar-Galán, S., and Francés, F.: Evaluation of ERA5 and ERA5-Land reanalysis precipitation datasets over Spain (1951–2020), Atmospheric Research, 284, 106 606, https://doi.org/10.1016/j.atmosres.2023.106606, 2023.

Gottardi, F.: Estimation statistique et réanalyse des précipitations en montagne
Utilisation d'ébauches par types de temps et assimila-

770 tion de données d'enneigement
Application aux grands massifs montagneux français, phdthesis, Institut National Polytechnique de Grenoble - INPG, https://tel.archives-ouvertes.fr/tel-00419170, 2009.

Groisman, P. Y. and Legates, D. R.: The Accuracy of United States Precipitation Data, Bulletin of the American Meteorological Society, 75, 215–228, https://doi.org/10.1175/1520-0477(1994)075<0215:TAOUSP>2.0.CO;2, publisher: American Meteorological Society Section: Bulletin of the American Meteorological Society, 1994.

775 Gössling, S., Peeters, P., Hall, C. M., Ceron, J.-P., Dubois, G., Lehmann, L. V., and Scott, D.: Tourism and water use: Supply, demand, and security. An international review, Tourism Management, 33, 1–15, https://doi.org/10.1016/j.tourman.2011.03.015, 2012.

Hassler, B. and Lauer, A.: Comparison of Reanalysis and Observational Precipitation Datasets Including ERA5 and WFDE5, Atmosphere, 12, 1462, https://doi.org/10.3390/atmos12111462, number: 11 Publisher: Multidisciplinary Digital Publishing Institute, 2021.

Hofstra, N., New, M., and McSweeney, C.: The influence of interpolation and station network density on the distributions and trends of

780 climate variables in gridded daily data, Climate Dynamics, 35, 841–858, https://doi.org/10.1007/s00382-009-0698-1, 2010.

Hohenegger, C., Brockhaus, P., and Schär, C.: Towards climate simulations at cloud-resolving scales, Meteorologische Zeitschrift, pp. 383–394, https://doi.org/10.1127/0941-2948/2008/0303, publisher: Schweizerbart'sche Verlagsbuchhandlung, 2008.

Huang, W.-R., Liu, P.-Y., and Hsu, J.: Multiple timescale assessment of wet season precipitation estimation over Taiwan us-ing the PERSIANN family products, International Journal of Applied Earth Observation and Geoinformation, 103, 102 521,

785 https://doi.org/10.1016/j.jag.2021.102521, 2021.

Jiang, Q.: Moist dynamics and orographic precipitation, Tellus A: Dynamic Meteorology and Oceanography, 55, 301, https://doi.org/10.3402/tellusa.v55i4.14577, number: 4 Publisher: Stockholm University Press, 2003.

Jiang, Y., Yang, K., Shao, C., Zhou, X., Zhao, L., Chen, Y., and Wu, H.: A downscaling approach for constructing high-resolution precipitation dataset over the Tibetan Plateau from ERA5 reanalysis, Atmospheric Research, 256, 105 574, https://doi.org/10.1016/j.atmosres.2021.105574, 2021.

Jiang, Y., Yang, K., Yang, H., Lu, H., Chen, Y., Zhou, X., Sun, J., Yang, Y., and Wang, Y.: Characterizing basin-scale precipitation gradients in the Third Pole region using a high-resolution atmospheric simulation-based dataset, Hydrology and Earth System Sciences, 26, 4587–4601, https://doi.org/10.5194/hess-26-4587-2022, publisher: Copernicus GmbH, 2022.

Kass, R. E. and Raftery, A. E.: Bayes Factors, Journal of the American Statistical Association, 90, 773–795, https://doi.org/10.1080/01621459.1995.10476572, publisher: Taylor & Francis _eprint: https://www.tandfonline.com/doi/pdf/10.1080/01621459.1995.10476572, 1995.

Kendon, E. J., Roberts, N. M., Senior, C. A., and Roberts, M. J.: Realism of Rainfall in a Very High-Resolution Regional Climate Model, Journal of Climate, 25, 5791–5806, https://doi.org/10.1175/JCLI-D-11-00562.1, publisher: American Meteorological Society Section: Journal of Climate, 2012.

Keuler, K., Radtke, K., Kotlarski, S., and Lüthi, D.: Regional climate change over Europe in COSMO-CLM: Influence of emission scenario and driving global model, Meteorologische Zeitschrift, pp. 121–136, https://doi.org/10.1127/metz/2016/0662, publisher: Schweizerbart'sche Verlagsbuchhandlung, 2016.

Kotlarski, S., Bosshard, T., Lüthi, D., Pall, P., and Schär, C.: Elevation gradients of European climate change in the regional climate model COSMO-CLM, Climatic Change, 112, 189–215, https://doi.org/10.1007/s10584-011-0195-5, 2012.

Kumar, B., Roy, D., and Lakshmi, V.: Impact of temperature and precipitation lapse rate on hydrological modelling over Himalayan Gandak River Basin, Journal of Mountain Science, 19, 3487–3502, https://doi.org/10.1007/s11629-020-6602-5, 2022.

Le Moigne, P.: Documentation of the CERRA-Land system, Tech. rep., Météo-France, 2021.

Li, L., Gochis, D. J., Sobolowski, S., and Mesquita, M. D. S.: Evaluating the present annual water budget of a Himalayan headwater river basin using a high-resolution atmosphere-hydrology model, Journal of Geophysical Research: Atmospheres, 122, 4786–4807, https://doi.org/10.1002/2016JD026279, _eprint: https://onlinelibrary.wiley.com/doi/pdf/10.1002/2016JD026279, 2017.

Lucas-Picher, P., Argüeso, D., Brisson, E., Tramblay, Y., Berg, P., Lemonsu, A., Kotlarski, S., and Caillaud, C.: Convection-permitting modeling with regional climate models: Latest developments and next steps, WIREs Climate Change, 12, e731, https://doi.org/10.1002/wcc.731, _eprint: https://onlinelibrary.wiley.com/doi/pdf/10.1002/wcc.731, 2021.

Lundquist, J., Hughes, M., Gutmann, E., and Kapnick, S.: Our skill in modeling mountain rain and snow is bypassing the skill of our observational networks, Bulletin of the American Meteorological Society, pp. 2473–2490, https://doi.org/10.1175/BAMS-D-19-0001.1, 2019.

Mahmood, T. H., Putkonen, J., and Sobbe, A.: Spatially Variable Precipitation and Its Influence on Water Balance in a Headwater Alpine Basin, Nepal, Water, 13, 254, https://doi.org/10.3390/w13030254, number: 3 Publisher: Multidisciplinary Digital Publishing Institute, 2021.

Markstrom, S. L., Regan, R. S., Hay, L. E., Viger, R. J., Webb, R. M., Payn, R. A., and LaFontaine, J. H.: PRMS-IV, the precipitation-runoff modeling system, version 4, Tech. rep., US Geological Survey, 2015.

Mestre, O., Domonkos, P., Picard, F., Auer, I., Robin, S., Lebarbier, E., Böhm, R., Aguilar, E., Guijarro Pastor, J. A., Vertacnik, G., Klancar, M., Dubuisson, B., and Stepanek, P.: HOMER: a homogenization software – methods and applications, Idojaras, https://repositorio.aemet.es/handle/20.500.11765/1494, accepted: 2016-03-29T12:17:14Z Company: Agencia Estatal de Meteorología Distrib-

825   utor: Agencia Estatal de Meteorología Institution: Agencia Estatal de Meteorología Label: Agencia Estatal de Meteorología Publisher: Hungarian Meteorological Service, 2013.

Monteiro, D., Caillaud, C., Samacoïts, R., Lafaysse, M., and Morin, S.: Potential and limitations of convection-permitting CNRM-AROME climate modelling in the French Alps, International Journal of Climatology, 42, 7162–7185, https://doi.org/10.1002/joc.7637, 2022.

830   Mott, R., Scipión, D., Schneebeli, M., Dawes, N., Berne, A., and Lehning, M.: Orographic effects on snow deposition patterns in mountainous terrain, Journal of Geophysical Research: Atmospheres, 119, 1419–1439, https://doi.org/10.1002/2013JD019880, _eprint: https://onlinelibrary.wiley.com/doi/pdf/10.1002/2013JD019880, 2014.

Muggeo, V. M.: segmented: an R Package to Fit Regression Models with Broken-Line Relationships., R News, 8, 20–25, https://cran.r-project.org/doc/Rnews/, 2008.

835   Muñoz-Sabater, J., Dutra, E., Agustí-Panareda, A., Albergel, C., Arduini, G., Balsamo, G., Boussetta, S., Choulga, M., Harrigan, S., Hersbach, H., Martens, B., Miralles, D. G., Piles, M., Rodríguez-Fernández, N. J., Zsoter, E., Buontempo, C., and Thépaut, J.-N.: ERA5-Land: a state-of-the-art global reanalysis dataset for land applications, Earth System Science Data, 13, 4349–4383, https://doi.org/10.5194/essd-13-4349-2021, 2021.

Ménégoz, M., Valla, E., Jourdain, N. C., Blanchet, J., Beaumet, J., Wilhelm, B., Gallée, H., Fettweis, X., Morin, S., and Anquetin, S.:
840   Contrasting seasonal changes in total and intense precipitation in the European Alps from 1903 to 2010, Hydrology and Earth System Sciences, 24, 5355–5377, https://doi.org/10.5194/hess-24-5355-2020, publisher: Copernicus GmbH, 2020.

Napoli, A., Crespi, A., Ragone, F., Maugeri, M., and Pasquero, C.: Variability of orographic enhancement of precipitation in the Alpine region, Scientific Reports, 9, 13 352, https://doi.org/10.1038/s41598-019-49974-5, 2019.

Nguyen, P., Ombadi, M., Gorooh, V. A., Shearer, E. J., Sadeghi, M., Sorooshian, S., Hsu, K., Bolvin, D., and Ralph, M. F.: PERSIANN Dy-
845   namic Infrared–Rain Rate (PDIR-Now): A Near-Real-Time, Quasi-Global Satellite Precipitation Dataset, Journal of Hydrometeorology, 21, 2893–2906, https://doi.org/10.1175/JHM-D-20-0177.1, publisher: American Meteorological Society Section: Journal of Hydrometeorology, 2020.

Nie, S., Luo, Y., Wu, T., Shi, X., and Wang, Z.: A merging scheme for constructing daily precipitation analyses based on objective bias-correction and error estimation techniques, Journal of Geophysical Research: Atmospheres, 120, 8671–8692,
850   https://doi.org/10.1002/2015JD023347, _eprint: https://onlinelibrary.wiley.com/doi/pdf/10.1002/2015JD023347, 2015.

Ochoa-Rodriguez, S., Wang, L.-P., Willems, P., and Onof, C.: A Review of Radar-Rain Gauge Data Merging Methods and Their Potential for Urban Hydrological Applications, Water Resources Research, 55, 6356–6391, https://doi.org/10.1029/2018WR023332, 2019.

Ogrin, M. and Kozamernik, E.: Horizontal Precipitation Gradients in Alpine Valleys of Northwestern Slovenia, Dela, pp. 5–36, https://doi.org/10.4312/dela.49.5-36, number: 49, 2018.

855   Ogrin, M. and Kozamernik, E.: Vertical precipitation gradients: a case study of Alpine valleys of northwestern Slovenia, Theoretical and Applied Climatology, 140, 401–409, https://doi.org/10.1007/s00704-019-03051-z, 2020.

Oudin, L., Perrin, C., Mathevet, T., Andréassian, V., and Michel, C.: Impact of biased and randomly corrupted inputs on the efficiency and the parameters of watershed models, Journal of Hydrology, 320, 62–83, https://doi.org/10.1016/j.jhydrol.2005.07.016, 2006.

Pahaut, E.: L'organisation de la prevision du risque d'avalanches en France, Tech. rep., Météo-France, Toulouse, 77 p., 1991.

860   Panziera, L., James, C. N., and Germann, U.: Mesoscale organization and structure of orographic precipitation producing flash floods in the Lago Maggiore region, Quarterly Journal of the Royal Meteorological Society, 141, 224–248, https://doi.org/10.1002/qj.2351, _eprint: https://onlinelibrary.wiley.com/doi/pdf/10.1002/qj.2351, 2015.

Pimentel, D., Houser, J., Preiss, E., White, O., Fang, H., Mesnick, L., Barsky, T., Tariche, S., Schreck, J., and Alpert, S.: Water Resources: Agriculture, the Environment, and Society, BioScience, 47, 97–106, https://doi.org/10.2307/1313020, publisher: [American Institute of Biological Sciences, Oxford University Press], 1997.

Pollock, M. D., O'Donnell, G., Quinn, P., Dutton, M., Black, A., Wilkinson, M. E., Colli, M., Stagnaro, M., Lanza, L. G., Lewis, E., Kilsby, C. G., and O'Connell, P. E.: Quantifying and Mitigating Wind-Induced Undercatch in Rainfall Measurements, Water Resources Research, 54, 3863–3875, https://doi.org/10.1029/2017WR022421, _eprint: https://onlinelibrary.wiley.com/doi/pdf/10.1029/2017WR022421, 2018.

Ragettli, S. and Pellicciotti, F.: Calibration of a physically based, spatially distributed hydrological model in a glacierized basin: On the use of knowledge from glaciometeorological processes to constrain model parameters, Water Resources Research, 48, https://doi.org/10.1029/2011WR010559, _eprint: https://onlinelibrary.wiley.com/doi/pdf/10.1029/2011WR010559, 2012.

Rockel, B., Will, A., and Hense, A.: The Regional Climate Model COSMO-CLM (CCLM), Meteorologische Zeitschrift, pp. 347–348, https://doi.org/10.1127/0941-2948/2008/0309, publisher: Schweizerbart'sche Verlagsbuchhandlung, 2008.

Roger, L.: Validation et utilisation climatologiques de la ré-analyse de lame d'eau radar Comephore étendue, Stage de fin d'étude, Météo-France, Toulouse, 77 p., 2017.

Rouzeau, S.: Validation climatologique de la réanalyse lame d'eau Comephore 1997-2006, Stage de fin d'étude, Météo-France, Toulouse, 2013.

Ruelland, D.: Should altitudinal gradients of temperature and precipitation inputs be inferred from key parameters in snow-hydrological models?, Hydrology and Earth System Sciences, 24, 2609–2632, https://doi.org/10.5194/hess-24-2609-2020, publisher: Copernicus GmbH, 2020.

Sandre: Bassins versant topographiques - Métropole 2019 - BD Topage®, https://geo.data.gouv.fr/fr/datasets/06431249ccb898a370cdacba02347d2f5f0e2d77, 2020.

Schermerhorn: Relations between topography and annual precipitation in western Oregon and Washington, Water Resources Research, https://agupubs.onlinelibrary.wiley.com/doi/abs/10.1029/WR003i003p00707, 1967.

Schäppi, B.: Measurement and analysis of rainfall gradients along a hillslope transect in the Swiss Alps, Ph.D. thesis, ETH Zurich, https://doi.org/10.3929/ETHZ-A-009913260, artwork Size: 188 p. Medium: application/pdf Pages: 188 p., 2013.

Seity, Y., Brousseau, P., Malardel, S., Hello, G., Bénard, P., Bouttier, F., Lac, C., and Masson, V.: The AROME-France Convective-Scale Operational Model, Monthly Weather Review, 139, 976–991, https://doi.org/10.1175/2010MWR3425.1, publisher: American Meteorological Society Section: Monthly Weather Review, 2011.

Sevruk, B.: Regional dependency of precipitation-altitude relationship in the Swiss Alps, Climatic Change, 36, 355–369, https://doi.org/10.1023/A:1005302626066, 1997.

Sevruk, B. and Mieglitz, K.: The effect of topography, season and weather situation on daily precipitation gradients in 60 Swiss valleys, Water science and technology : a journal of the International Association on Water Pollution Research, 45, 41–8, https://doi.org/10.2166/wst.2002.0025, 2002.

Shen, Y., Hong, Z., Pan, Y., Yu, J., and Maguire, L.: China's 1 km Merged Gauge, Radar and Satellite Experimental Precipitation Dataset, Remote Sensing, 10, 264, https://doi.org/10.3390/rs10020264, number: 2 Publisher: Multidisciplinary Digital Publishing Institute, 2018.

Silverman, N. L., Maneta, M. P., Chen, S.-H., and Harper, J. T.: Dynamically downscaled winter precipitation over complex terrain of the Central Rockies of Western Montana, USA, Water Resources Research, 49, 458–470, https://doi.org/10.1029/2012WR012874, _eprint: https://onlinelibrary.wiley.com/doi/pdf/10.1029/2012WR012874, 2013.

900 Smith, R. B.: The Influence of Mountains on the Atmosphere, in: Advances in Geophysics, edited by Saltzman, B., vol. 21, pp. 87–230, Elsevier, https://doi.org/10.1016/S0065-2687(08)60262-9, 1979.

Soci, C., Bazile, E., Besson, F., and Landelius, T.: High-resolution precipitation re-analysis system for climatological purposes, Tellus A: Dynamic Meteorology and Oceanography, 68, 29 879, https://doi.org/10.3402/tellusa.v68.29879, publisher: Taylor & Francis _eprint: https://doi.org/10.3402/tellusa.v68.29879, 2016.

905 Spreen: A determination of the effect of topography upon precipitation, Eos, Transactions American Geophysical Union, 28, 285–290, https://doi.org/10.1029/TR028i002p00285, _eprint: https://onlinelibrary.wiley.com/doi/pdf/10.1029/TR028i002p00285, 1947.

Termonia, P., Fischer, C., Bazile, E., Bouyssel, F., Brožková, R., Bénard, P., Bochenek, B., Degrauwe, D., Derková, M., El Khatib, R., Hamdi, R., Mašek, J., Pottier, P., Pristov, N., Seity, Y., Smolíková, P., Španiel, O., Tudor, M., Wang, Y., Wittmann, C., and Joly, A.: The ALADIN System and its canonical model configurations AROME CY41T1 and ALARO CY40T1, Geoscientific Model Development, 11, 257–281,

910 https://doi.org/10.5194/gmd-11-257-2018, publisher: Copernicus GmbH, 2018.

Uysal, G.: Product- and Hydro-Validation of Satellite-Based Precipitation Data Sets for a Poorly Gauged Snow-Fed Basin in Turkey, Water, 14, 2758, https://doi.org/10.3390/w14172758, number: 17 Publisher: Multidisciplinary Digital Publishing Institute, 2022.

Viviroli, D., Dürr, H. H., Messerli, B., Meybeck, M., and Weingartner, R.: Mountains of the world, water towers for humanity: Typology, mapping, and global significance, Water Resources Research, 43, https://doi.org/10.1029/2006WR005653, _eprint:

915 https://onlinelibrary.wiley.com/doi/pdf/10.1029/2006WR005653, 2007.

Wrzesien, M. L., Pavelsky, T. M., Durand, M. T., Dozier, J., and Lundquist, J. D.: Characterizing Biases in Mountain Snow Accumulation From Global Data Sets, Water Resources Research, 55, 9873–9891, https://doi.org/10.1029/2019WR025350, _eprint: https://onlinelibrary.wiley.com/doi/pdf/10.1029/2019WR025350, 2019.
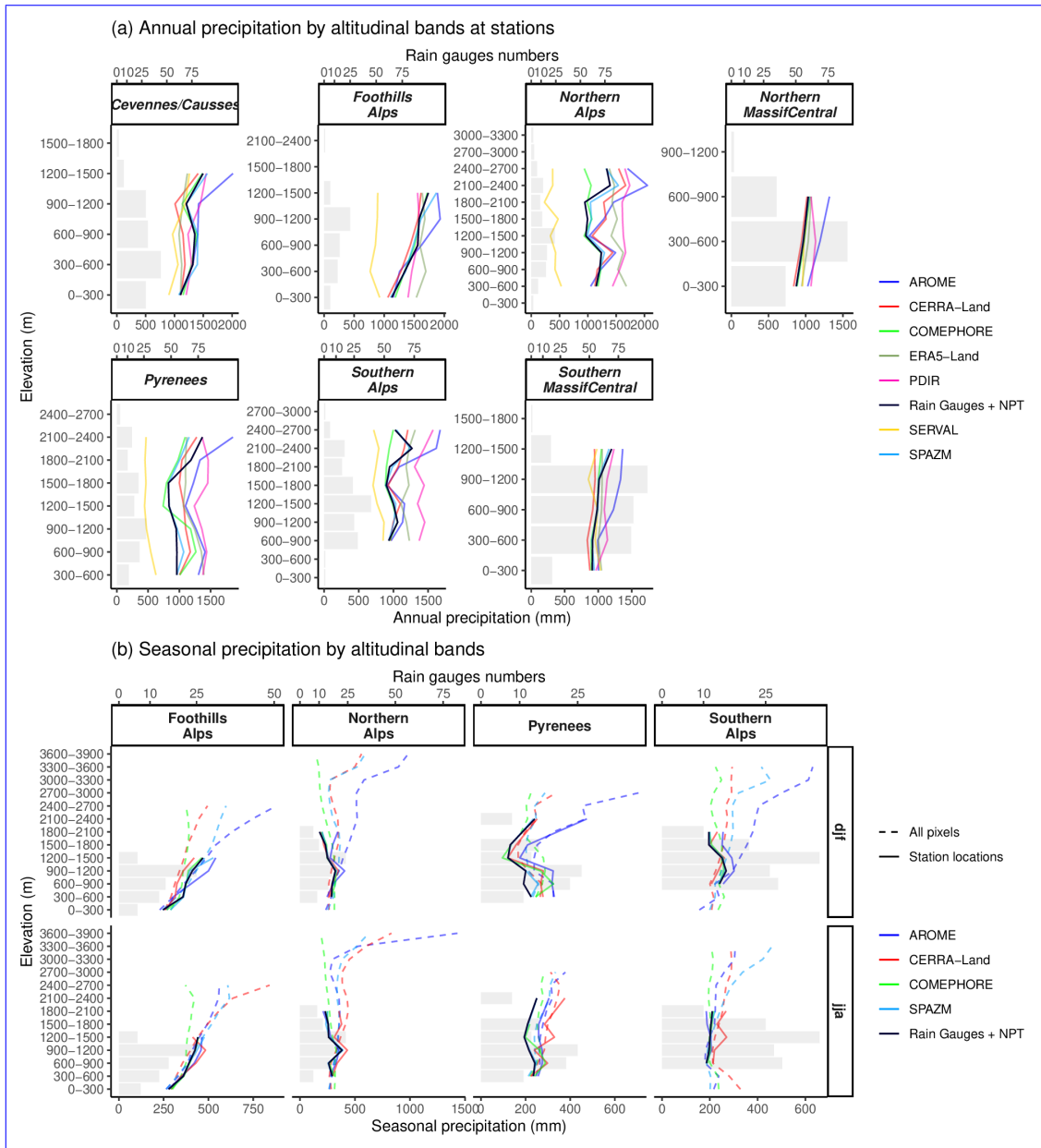
Figure 3. Comparison between the altitude dependence of precipitation from AROME, CERRA-Land, COMEPHORE, ERA5-Land, PDIR, SERVAL, SPAZM, stations (rain gauges and NPT) in seven regions. The lines show the median precipitation amount in each altitude zone and the bars denote the number of rain gauges in each area. Comparisons are done at **(a)** the station locations at the annual scale and **(b)** both station locations and on all pixels from the gridded products at the seasonal scale. At the seasonal scale, only AROME, CERRA-Land, COMEPHORE, and SPAZM are analyzed for the sake of visualization. The season *djf* refers to the winter (December, January, February) and the season *jja* corresponds to the summer (June, July, August).
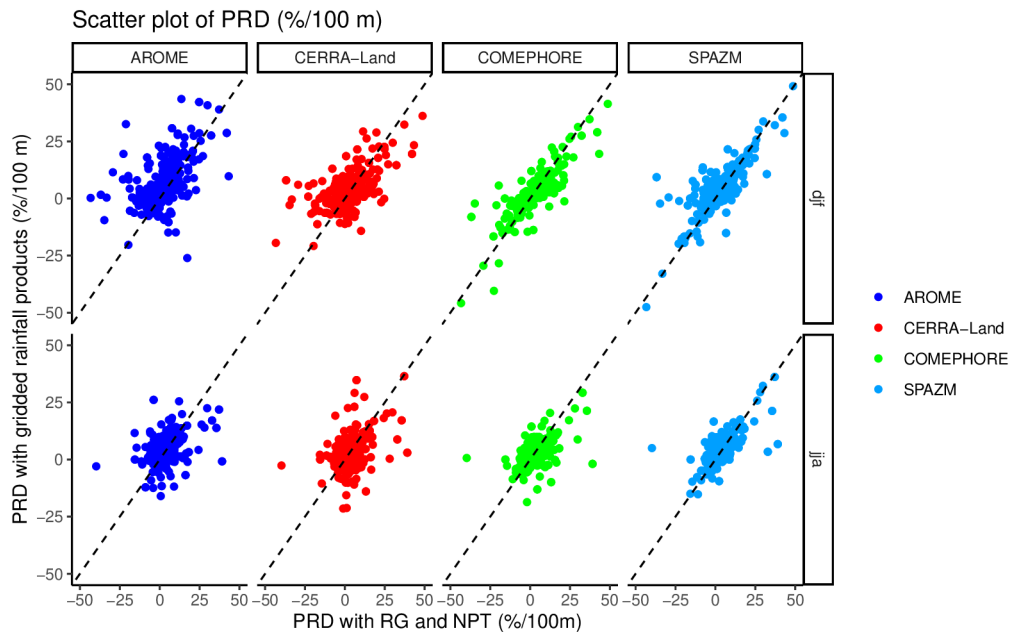
Figure 4. Comparison of precipitation relative difference (%/100 m) computed with stations and gridded rainfall products. PRDs are derived for all couples of neighboring stations. Scatter plot between observed and gridded PRD at station locations. The dotted lines indicate the 1:1 lines.
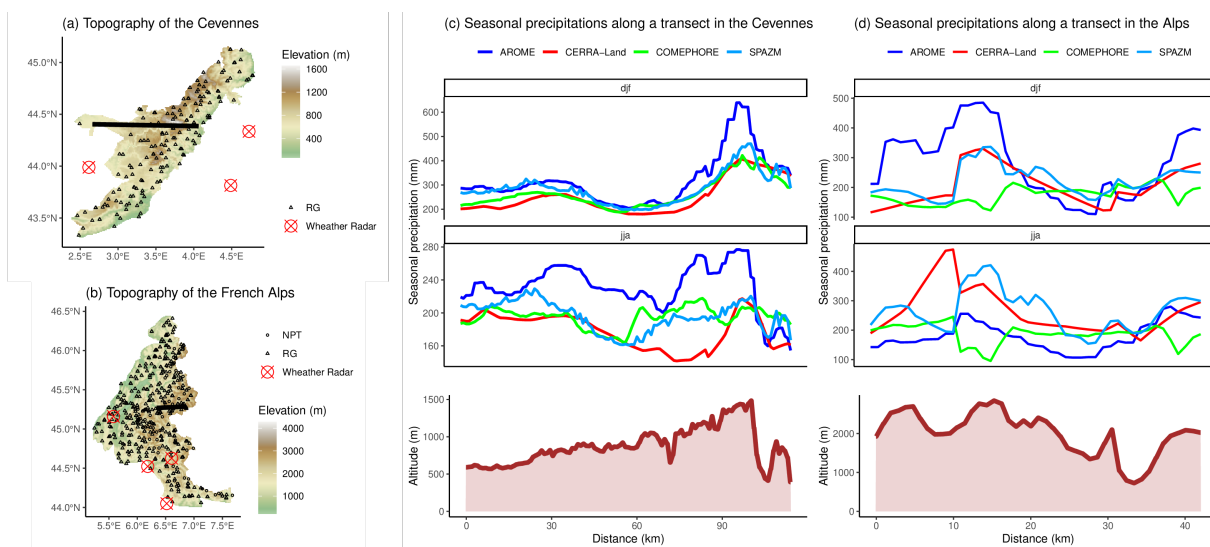
Figure 5. Transects in the Cévennes **(a)** and the Northern Alps **(b)**. Winter *djf* and summer *jja* precipitations extracted across the transects are colored according to gridded products **(c)**, **(d)**. Elevation is represented in brown as an altitude profile.
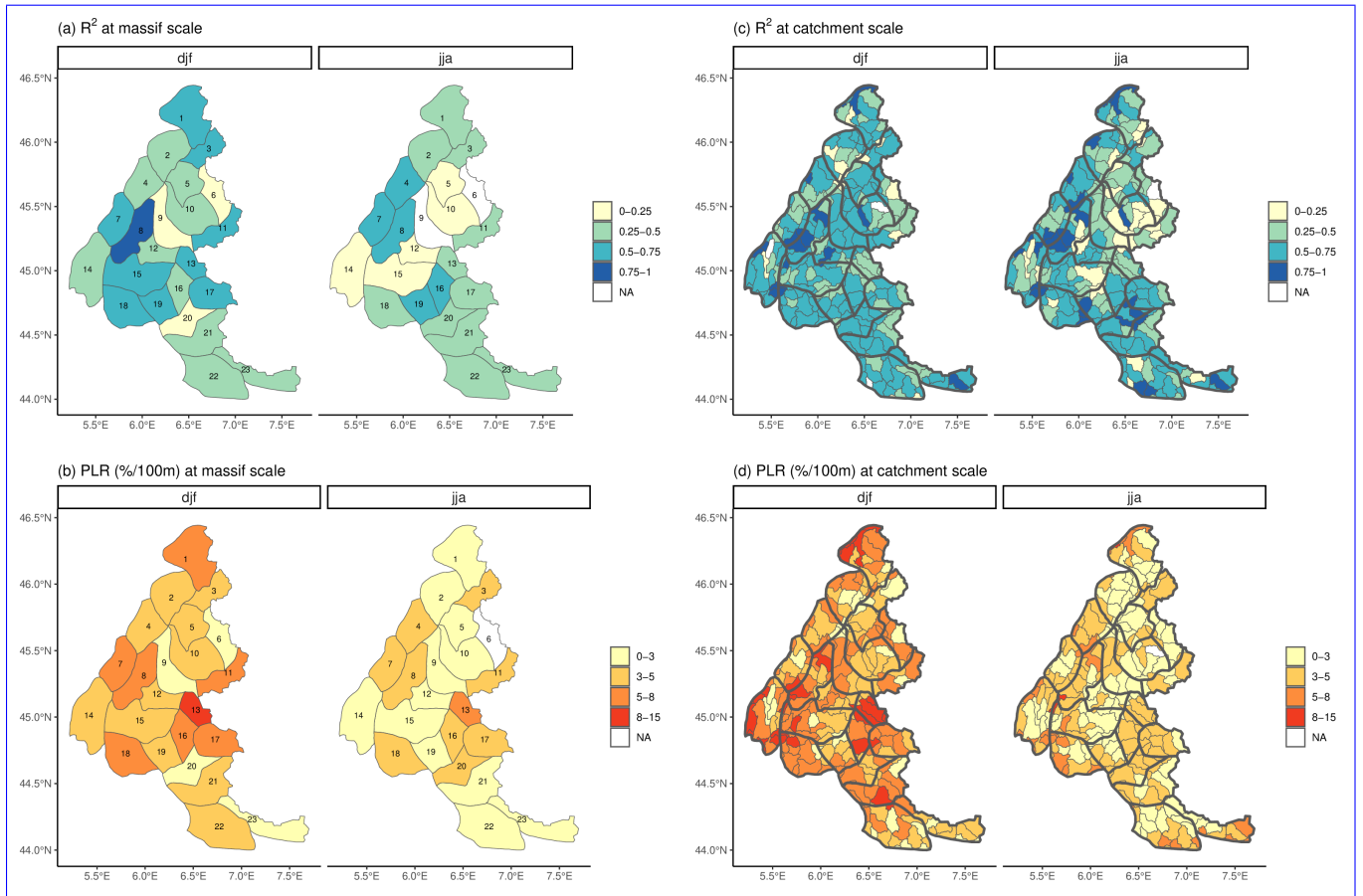
Figure 6. Spatial distribution of R^2 **(a), (c)** and precipitation lapse rates (precipitation change per 100 m altitude difference divided by area-average precipitation) **(b), (d)** extracted from the precipitation-altitude regressions for all grids within each area. Categorical results are displayed in the French Alps at regional and catchment scales for both winter *djf* and summer *jja* precipitations. The area indicated as "NA" and filled in white represents regions with insufficient altitudinal variability to compute precipitation gradient. The ~~names~~ indexes of the massifs ~~and their corresponding R^2 and precipitation gradient values~~ are also printed and refer to Table 3.
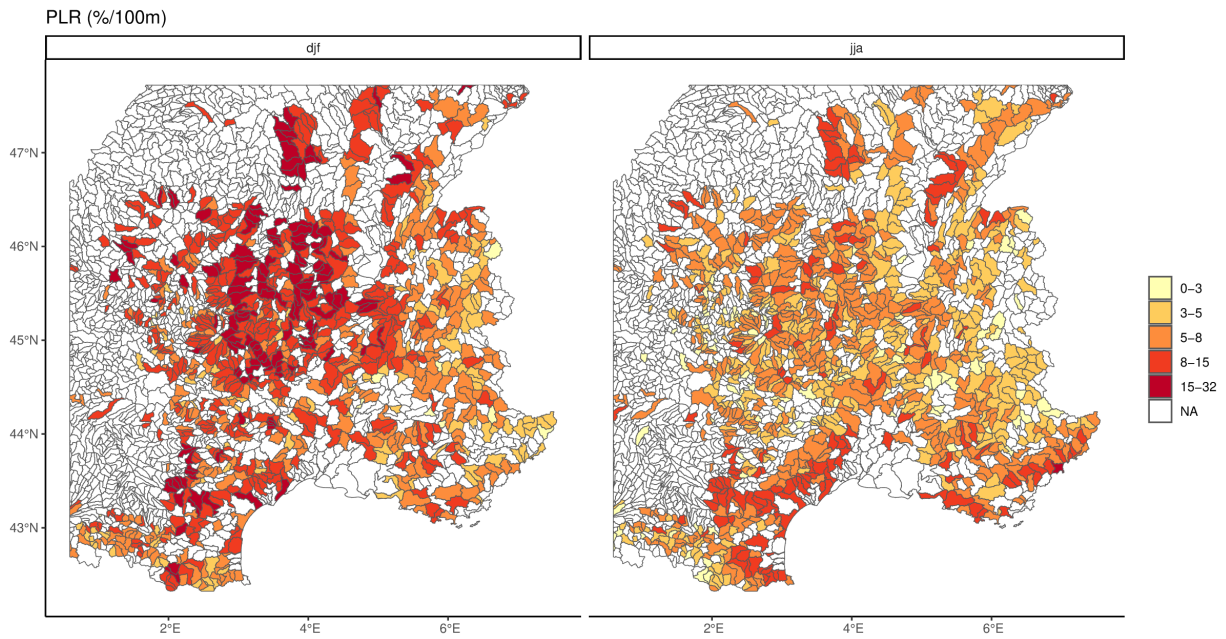
Figure 7. Spatial distribution of winter *djf* and summer *jja* precipitation lapse rates (precipitation change per 100 m altitude difference divided by area-averaged precipitation) extracted from the precipitation-altitude regressions for all grids within each area. Categorical results are displayed in the study domain at the catchment scale. The area indicated as "NA" and filled in white represents catchments with insufficient altitudinal variability (standard deviation of the altitude lower than 50 m) or R^2 inferior to 0.5.
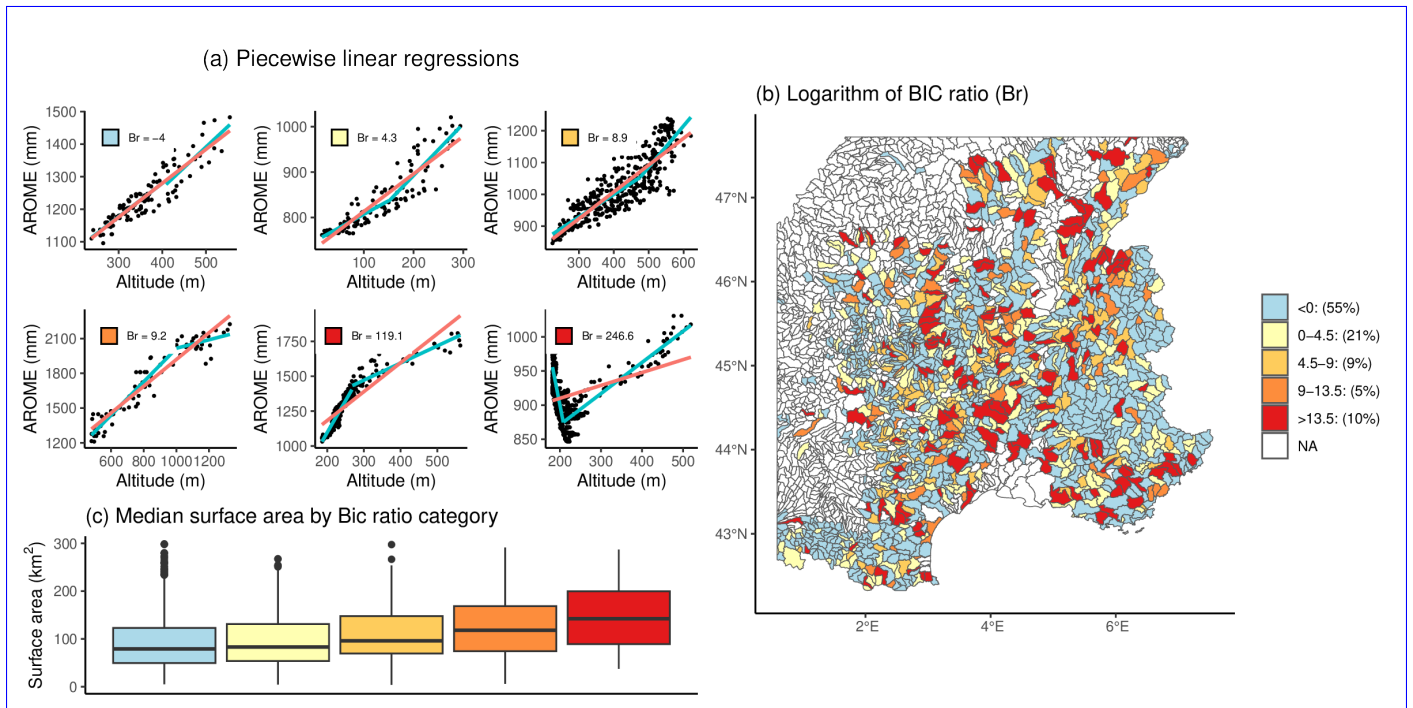
Figure 8. **(a)** Scatter plots of AROME annual precipitation (mm) as a function of the altitude for some catchments taken as illustrative examples of the different categories of BIC ratio. Linear (red lines) and piecewise linear (blue curves) regressions are superimposed. **(b)** Spatial representation of the logarithm of the BIC ratios between linear and piecewise linear regression (annual precipitation ∼ altitude) models. The numbers expressed in % correspond to the percentage of catchments within the classes of the BIC ratio. **(c)** Distribution of the surface area of the catchments according to the categories of BIC ratio.
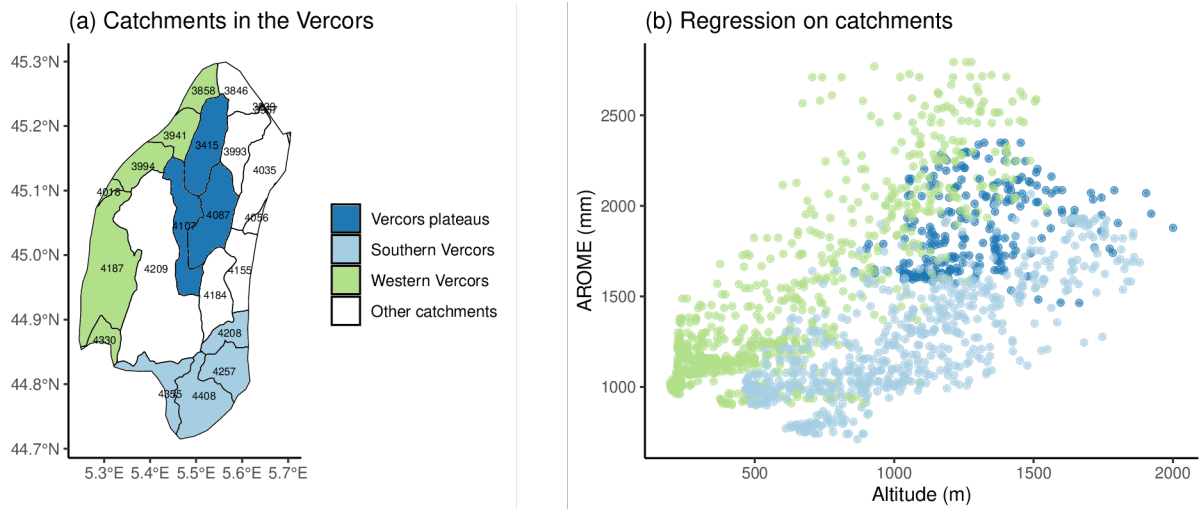
Figure 9. (a) Catchments located in the Vercors massif and colored according to their geographic locations. Three groups of catchments are distinguished: the Vercors plateaus, the Western Vercors, and the Southern Vercors. ID numbers are printed for each catchment. **(b)** Scatter plot of AROME annual precipitation and altitude for the pixels in the Vercors (gray dots). The colors of dots correspond to the colors used in panel a).